UNIVERSIDAD DE INVESTIGACIÓN DE TECNOLOGÍA EXPERIMENTAL YACHAY

Escuela de Ciencias Físicas y Nanotecnología

TÍTULO: Structural characterization and electrochemical properties of natural carbon fibers decorated with nanoparticles

Trabajo de integración curricular presentado como requisito para la obtención del título de Físico

Autor:

Gaona Torres Steven Javier

Tutor:

PhD. González Vásquez Gema

Cotutores:

PhD. Briceño Sarah
MSc. Corredor Luis

Urcuquí, Junio 2021

SECRETARÍA GENERAL
(Vicerrectorado Académico/Cancillería)
ESCUELA DE CIENCIAS FÍSICAS Y NANOTECNOLOGÍA
CARRERA DE FÍSICA
ACTA DE DEFENSA No. UITEY-PHY-2021-00013-AD

A los 11 días del mes de junio de 2021, a las 15:00 horas, de manera virtual mediante videoconferencia, y ante el Tribunal Calificador, integrado por los docentes:

Presidente Tribunal de Defensa	Dr. BRAMER ESCAMILLA , WERNER , Ph.D.
Miembro No Tutor	Dr. AVILA SOSA, EDWARD EBNER , Ph.D.
Tutor	Dra. GONZALEZ VAZQUEZ, GEMA , Ph.D.

El(la) señor(ita) estudiante **GAONA TORRES, STEVEN JAVIER**, con cédula de identidad No. **1723041321**, de la **ESCUELA DE CIENCIAS FÍSICAS Y NANOTECNOLOGÍA**, de la Carrera de **FÍSICA**, aprobada por el Consejo de Educación Superior (CES), mediante Resolución **RPC-SO-39-No.456-2014**, realiza a través de videoconferencia, la sustentación de su trabajo de titulación denominado: **Structural Characterization and electrochemical properties of natural carbon fibers decorated with nanoparticles**, previa a la obtención del título de **FÍSICO/A**.

El citado trabajo de titulación, fue debidamente aprobado por el(los) docente(s):

Tutor	Dra. GONZALEZ VAZQUEZ, GEMA , Ph.D.
Co - Tutor	Dra. BRICEÑO ARAUJO, SARAH ELISA , Ph.D.
Co - Tutor	MSC CORREDOR GONZALEZ, LUIS GERARDO

Y recibió las observaciones de los otros miembros del Tribunal Calificador, las mismas que han sido incorporadas por el(la) estudiante.

Previamente cumplidos los requisitos legales y reglamentarios, el trabajo de titulación fue sustentado por el(la) estudiante y examinado por los miembros del Tribunal Calificador. Escuchada la sustentación del trabajo de titulación a través de videoconferencia, que integró la exposición de el(la) estudiante sobre el contenido de la misma y las preguntas formuladas por los miembros del Tribunal, se califica la sustentación del trabajo de titulación con las siguientes calificaciones:

Tipo	Docente	Calificación
Tutor	Dra. GONZALEZ VAZQUEZ, GEMA , Ph.D.	10,0
Miembro Tribunal De Defensa	Dr. AVILA SOSA, EDWARD EBNER , Ph.D.	10,0
Presidente Tribunal De Defensa	Dr. BRAMER ESCAMILLA , WERNER , Ph.D.	10,0

Lo que da un promedio de: **10 (Diez punto Cero)**, sobre 10 (diez), equivalente a: **APROBADO**

Para constancia de lo actuado, firman los miembros del Tribunal Calificador, el/la estudiante y el/la secretario ad-hoc.

Certifico que *en cumplimiento del Decreto Ejecutivo 1017 de 16 de marzo de 2020, la defensa de trabajo de titulación (o examen de grado modalidad teórico práctica) se realizó vía virtual, por lo que las firmas de los miembros del Tribunal de Defensa de Grado, constan en forma digital.*

GAONA TORRES, STEVEN JAVIER
Estudiante

Dr. BRAMER ESCAMILLA , WERNER , Ph.D.
Presidente Tribunal de Defensa

Firmado electrónicamente por:
WERNER BRAMER

Dra. GONZALEZ VAZQUEZ, GEMA , Ph.D.
Tutor

Firmado electrónicamente por:
GEMA GONZALEZ

Dr. AVILA   SOSA, EDWARD EBNER , Ph.D.
Miembro No Tutor

EDWARD EBNER AVILA SOSA

Digitally signed by EDWARD EBNER AVILA SOSA
Date: 2021.06.11 16:22:23 -05'00'

CIFUENTES TAFUR, EVELYN CAROLINA
Secretario Ad-hoc

Firmado electrónicamente por:
EVELYN CAROLINA CIFUENTES TAFUR

AUTORÍA

Yo, **STEVEN JAVIER GAONA TORRES**, con cédula de identidad 1723041321, declaro que las ideas, juicios, valoraciones, interpretaciones, consultas bibliográficas, definiciones y conceptualizaciones expuestas en el presente trabajo; así cómo, los procedimientos y herramientas utilizadas en la investigación, son de absoluta responsabilidad de el/la autora (a) del trabajo de integración curricular. Así mismo, me acojo a los reglamentos internos de la Universidad de Investigación de Tecnología Experimental Yachay.

Urcuquí, junio 2021.

_____

Steven Javier Gaona Torres
CI: 1723041321

AUTORIZACIÓN DE PUBLICACIÓN

Yo, **STEVEN JAVIER GAONA TORRES,** con cédula de identidad 1723041321, cedo a la Universidad de Tecnología Experimental Yachay, los derechos de publicación de la presente obra, sin que deba haber un reconocimiento económico por este concepto. Declaro además que el texto del presente trabajo de titulación no podrá ser cedido a ninguna empresa editorial para su publicación u otros fines, sin contar previamente con la autorización escrita de la Universidad.

Asimismo, autorizo a la Universidad que realice la digitalización y publicación de este trabajo de integración curricular en el repositorio virtual, de conformidad a lo dispuesto en el Art. 144 de la Ley Orgánica de Educación Superior

Urcuquí, junio 2021.

_____

Steven Javier Gaona Torres
CI: 1723041321

To Eva, the age of the universe is about 14 billion years, the age of the earth is about 4.5 million years. The probability of existence and of having found you still seems to be completely null, but there you were when I needed it most. Thank you for teaching me that in the darkest night, there will always be a star of hope.

Steven J. Gaona Torres

Acknowledgements

I would like to thank my parents, Nely and Lauro, for their constant support, without you any of this could be possible. Dad, you taught me to never give up, thank you for believing in me, even when I didn't even do it myself, I am so grateful life put you by my side. Thanks to my family for being there asking about me, I love you all.

Special thanks to my advisor Ph.D. Gema Gonzalez. Learning from her has been a privilege. To my co-advisor Ph.D. Sarah Briceño, her guidance was crucial in the development of this work. I admire you both a lot, thank you so much for the inspiration. I am very grateful with MsC Luis Corredor, for your help with this work in the physics lab, and of course Evelyn Cifuentes who always was there (our dear dean). Thank you Ing. Darwin Mendez, for helping me with the creation of the mounting for the fibers. Thanks to Ph.D. Patricio Espinoza who allowed me to work in the PUCE lab, to Ing. Diego Bolaños from PUCE lab, who helped me and taught me all he knew about carbon fibers. I would like to thank Ph.D. Carlos Reinoso for his help with the XPS and for always being willing to help, people like you is what makes us love science.

Thanks to the Yachay Tech professors, you taught me to see the world with other eyes, it was an honor to receive lessons from all of you.

I thank all the wonderful people I met in Yachay Tech in these years. Stefano, my classmate, my best friend, I never understood how we became friends, but thank you for your support and truly friendship, the jokes, the sleepless nights while we were studying, that is just unforgettable.

Steven J. Gaona Torres

Resumen

El desarrollo de dispositivos de almacenamiento y energía respetuosos con el medio ambiente es de gran importancia en la actualidad. Entre estos, el desarrollo de fibras de Carbono (FC) a base de precursores de biomasa es de especial interés por el bajo costo de producción y las aplicaciones que se les pueden otorgar debido a la adición de nanopartículas que pueden afectar sus propiedades estructurales y electroquímicas. Este trabajo se centra en las fibras de carbono generadas a partir de recursos renovables. Los materiales de carbono han sido estudiados para diferentes aplicaciones debido a su excelente conductividad eléctrica, alta superficie y propiedades electroquímicas. Por lo tanto, se ha informado que los CF basados en biomasa son uno de los materiales más prometedores para su uso como electrodos y dispositivos de almacenamiento de energía. La incorporación de heteroátomos en la estructura del carbono es un enfoque eficaz para mejorar las propiedades electroquímicas. Las FC tienen un gran potencial para mejorar sus propiedades capacitivas al proporcionar una pseudocapacidad adicional y mejorar la superficie. humectabilidad y conductividad electrónica de los carbones. Actualmente, se ha reportado que los electrodos de FC basados en biomasa tienen una excelente respuesta capacitiva al tratarlos con KOH y $ZnCl_2$ como formadores de poros por el proceso de pirólisis, para ser aplicados como capacitores eléctricos de doble capa, así como electrodos fabricados con N-aerogel de fibra de carbono dopado. Buscando recursos más económicos para fabricar estos dispositivos basados en residuos naturales, el presente El trabajo propone la caracterización estructural y electroquímica de los residuos de fibras naturales de banano. Las fibras naturales de banano fueron pirolizadas y posteriormente dopadas con nanopartículas de Au, Ag, CeO_2, $CoFe_2O_4$ y Au / Fe_3O_4. Los materiales se caracterizaron por FTIR, XPS, SEM y voltamperometría cíclica. En general, el presente estudio presenta una nueva oportunidad para materiales nuevos, naturales y de bajo costo para aplicaciones de electrodos y capacitores.

Palabras clave: Fibras de carbono, Fibras de banano, Propiedades estructurales, Propiedades electroquímicas.

Abstract

The development of environmentally friendly energy and storage devices is of great importance nowadays.

Among these, the development of Carbon fibers (CFs) based on biomass precursors is of particular interest due to the low-cost of production and the applications that can be granted to them due to the addition of nanoparticles that can affect their structural and electrochemical properties. This work is focused on CFs generated from renewable resources. Carbon materials have been studied for different applications due to their excellent electrical conductivity, high surface area, and electrochemical properties. Thus, biomass-based CFs have been reported as one of the most promising materials for being used as electrodes and energy-storage devices. Incorporating heteroatoms into the carbon framework is an efficient approach for enhancing the electrochemical properties. CFs have a great potential for improving their capacitive properties by providing extra pseudo-capacitance and enhancing the surface wettability and carbons' electronic conductivity. Currently, biomass-based CFs electrodes have been reported to have an excellent capacitive response when treating them with KOH and $ZnCl_2$ as pore formers by the pyrolysis process, for being applied as electrical double-layer capacitors, as well as, electrodes fabricated from N-doped carbon fiber aerogel. Looking for more economical resources to fabricate these devices based on natural waste, the present work proposes the structural and electrochemical characterization of natural banana fibers waste. The natural banana fibers were pyrolyzed and subsequently doped with Au, Ag, CeO_2, $CoFe_2O_4$ and Au/Fe_3O_4 nanoparticles. The materials were characterized by FTIR, XPS, SEM, and cyclic voltammetry. Overall, the present study presents a new opportunity for low-cost, natural, and new materials for electrodes and capacitor applications.

Keywords: Carbon fibers, Banana fibers, Structural properties, Electrochemical properties

Contents

List of Figures

List of Tables

Chapter 1

Introduction

Over the last years, humans have been doing significant research, inventing and reinventing the world as we know it. This curiosity that our species have is what makes humans different from other animal species. The global growing of population, crisis of energy shortage, and environmental pollution caused by burning fossil fuels have brought about problems. They stimulate clean and sustainable energy, such as solar energy, wind power, and so on[1]. Moreover, for years, researchers have been trying to find the perfect material for specific applications. A particular area of interest is carbon fibers from biomass precursors in different applications, as electrodes, supercapacitors,etc.

A significant part of our life, we have learned that energy is the most important concept that keeps our world going forward. Thus, we know the necessity of Energy sources, and of course, the essential Energy storage. This last part is progressively crucial for various applications; in this area, batteries can store energy independently from the source (solar, wind, fossil, etc.). Supercapacitors' impact is remarkable; some authors define supercapacitor's concepts as Electrochemical capacitors (ECs) and emphasize that Supercapacitors are among the most promising energy storage devices. This because, once again, their excellent cyclability, high power density, and high charge and discharge rate[2].

Furthermore, the capability to mass manufacture electrochemical sensors at a low cost is a massive requirement for many applications and facilitates sensors' potential as disposable platforms. The wide range of potential applications has kept them as an object of study until today. Even modern electrochemical sensors are present in our daily lives, detecting several parameters, whether physical, chemical, or biological[3]. Some examples of electrochemical sensors' applications are sensors related to machines, sensors used in automobiles, environmental monitoring, and technology in general. The main objective of a chemical sensor is to provide reliable information in real-time, for instance, the chemical composition of its surrounding environment. Besides, the development of electrochemical sensors based on carbon fibers has been widely researched as an inexpensive method to detect a variety of biological analytes sensitively[4–6], and ideally, the final device will not perturb the sample[7].

Carbon fibers, along with carbon powders, carbon nanotubes, and graphene, can facilitate the creation of electrodes and the construction of electrical-double layer capacitors (EDLC) thanks to the properties they maintain[8]. In the research and development of carbon-based materials, a variety of biomass, such as oil palm empty fruit

bunches (EFB), rubberwood sawdust, and coconut husk, have been explored as possible precursors to produce activated carbon electrodes due to their large-scale availability, ease of processing, and relatively low cost[8].

Nowadays, most carbon fibers are manufactured from polyacrylonitrile (PAN) precursors while a small amount is derived from pitches, notably mesophase. However, due to the elevated cost of these petroleum-based precursors and the costs associated with the manufacturing process, carbon fibers use has been limited mainly to the aerospace and automotive industry, sporting goods, and specialist industrial applications[9]. In this way, one must remember that Ecuador is known globally as one of the biggest banana producers around the world, and one of the largest producers in the region along with Brazil, both countries with an average of 7 million tonnes[10], and therefore one of the countries with the largest plantations of this type.

Musa Paradisíaca constitutes one of the most important agricultural activities to the country's economy. In 2010, Ecuador exported approximately 4 million tons of bananas. During 2018, the total produced product was 7,157,603 tonnes[11,12]. Starting from here, the ease with which any person can obtain raw material (biomass precursor) for the manufacture of carbon fibers is really elevated.

The present thesis aims to use the pseudo-stem located "inside" the banana trunk, which is the most fibrous part of the plant, to extract the carbon fibers and doped them with different nanoparticles to study their potential for various applications. Besides, the overview would give us scope for improving materials based on carbon fibers. Also, it shows extraction, dried, pyrolyzed, functionalization, and then decoration of raw and pyrolyzed carbon fibers with Au, Ag, CeO_2, $CoFe_2O_4$, and Au/Fe_3O_4 nanoparticles; the fibers were tested by using SEM, RAMAN, XPS, FTIR, and cyclic voltammetry. The results are promising, since the behavior of CFs decorated with nanoparticles are similar to the behavior of studies performed on PAN-based CFs.

1.1 Problem Statement

The demand for CFs is increasing each year at a 10% rate and is expected to reach 89000 tons by 2020[13]. Those were the numbers until the last year. As the world continues its advance in science and technology, it is necessary to look at natural and renewable materials for obtaining fibers from natural precursors. Carbon fibers from banana trunk precursors seem to be a natural alternative eco-friendly material for this purpose. It must be said that over 98% of CFs are made from poly(acrylonitrile) (PAN) as a precursor[9,14–16]. PAN carbon-fiber was first recognized as an appropriate precursor material for CFs by Shindo in the late 1950s[17]. This material consists of extremely thin acrylic fibers, which are mostly made out of carbon atoms. With all the previous context, other sources (precursors) have been studied for the last decades to establish CFs in the mass market. The price of CFs has to be significantly reduced, and here is where low-cost CFs creation methods come into play. It is worth mentioning that in the review presented by Adeniyi, et al 2019. They observed that very little research attention has been paid to plantain fibers. Furthermore, they stated that also electrical (dielectric strength and electrical resistivity) and chemical properties of banana and plantain fiber composites have received very little attention[18].

Being Ecuador, a country with a very high Banana production level, it instantly is traduced into a high quantity of agro-industrial waste. It could be possible to handle the treatment of waste while obtaining technological value from it. Then, the possibilities of working with a natural biomass precursor and its economic impact make these fibers a robust tool for science and the Ecuadorian industry.

1.2 General and Specific Objectives

1.2.1 General Objective

To study the structure characterization and the properties of natural carbon fibers decorated with Au, Ag, CeO_2, $CoFe_2O_4$ and Au/Fe_3O_4 nanoparticles.

1.2.2 Specific Objectives

- Obtain and extract the fibers from a trunk sample of *Musa Paradisíaca* collected in the tropical area of Santo Domingo - Ecuador.

- Pyrolyze the extracted fibers as a function of temperature.

- Functionalize and decorate by immersion of the carbon fibers in Au, Ag, CeO_2, $CoFe_2O_4$ and Au/Fe_3O_4 nanoparticles media.

- Characterize the carbon fibers obtained using SEM, Raman, XPS, FTIR, and cyclic voltammetry.

Chapter 2

Theoretical Background

2.1 Nanotechnology

In 1959, Richard Feynman firstly revealed the conceptual bases regarding nanotechnology, although some properties of small materials were known from 1857 when Michael Faraday observed the interaction of light with metal nanoparticles[19,20].

Over the last decade, Nanotechnology has gained huge attention because it is an emerging field of science in which the synthesis and development of various nanomaterials is involved. Nanotechnology refers to the creation and application of materials whose constituents exist at the nanoscale. By convention, nanoparticles (NPs) are particles between 1 and 100 nanometers in size and can be made up of metal oxides, metal, carbon, or organic matter. The nanoparticles exhibit a unique structural, electrical, optical, and magnetic activity as well as chemical and biological properties at nanoscale compared to the bulk material.

Nanoparticles are being used for diverse purposes nowadays, from medical treatments as well to industrial products such as solar and oxide fuel batteries for energy storage. Due to the exceptional properties of NPS, including antibacterial activity (e.g, Ag NPs), high resistance to oxidation, and high thermal conductivity, nanoparticles have attracted considerable attention in recent years. Nanoparticles can be synthesized chemically or biologically. Metallic nanoparticles that have immense applications in industries are of different types, namely, Gold, Silver, Alloy, magnetic, etc[21,22].

A nanoparticle can be either zero-dimensional where the length, breadth, and height is fixed at a single point, for example, nanodots, one dimensional where it can possess only one parameter, for example, carbon nanotubes, two dimensional where it has length and breadth, for example, graphene or three dimensional where it has all the parameters: breadth, length, and height, for example, gold nanoparticles. NPs can have different shapes, sizes, and structures. NPs can be cylindrical, spherical, conical, hollow core, tubular, flat, spiral, etc., or irregular and differ from 1 nm to 100 nm in size. Surface variations may make the surface uniform or irregular. Some nanoparticles are crystalline or amorphous, with loose or agglomerated single or multi-crystal solids.[23].

2.2   State of Art

Numerous different polymers have been researched as biomass-based carbon fibers (BBCFs) forerunners[24]. Some even depend on the location where the research is carried out. For example Brazil, in this area, a lot of eucalyptus wood is pyrolyzed for charcoal production. Given that most Brazilian charcoal production uses wood from planted eucalyptus forests, then the importance of giving biomass a value-added turns it into an environmentally friendly activity. So in the pyrolysis process, the volatiles released can be recovered by condensation to give rise to an oily liquid called wood tar which is separated by decanting to give rise to an aqueous fraction (so-called pyroligneous acid) and an organic fraction (insoluble tar), which corresponds to around 35% and 7% of the initial mass of wood, respectively. Despite using insoluble tar as flavors, fragrances, and sources of fine chemical products, a heavier fraction, the so-called wood tar pitch, is then obtained as a distillation residue (about 50% in mass)[25].

Prauchner et al. in 2005 reported the eucalyptus tar pitches as precursors of general-purpose carbon fibers (GPCF) through carbonization. Their work aimed to characterize eucalyptus tar pitch and investigate its potential uses. In their work, they obtained and pyrolyzed fibers at 1000 °C (2.0 °C/min; 1 h) under nitrogen atmosphere in a stainless steel tubular furnace, achieving fibers that are not so strong for structural uses, but electrical properties came to light[25].

In 2007, Subramanian et al. successfully obtained carbons from banana fibers treated with KOH and $ZnCl_2$ as pore formers by the simple pyrolysis process, making the synthesis and activation processes eco-friendly. They showed that the activated carbon suffered an enhancement in surface area of up to 30 times than the untreated one. Different particle structures, morphology, and surface area are greatly reflected in the high-rate long-cycle electrochemical performance. The specific capacitance of the carbon material treated with $ZnCl_2$ showed the best performance with a value of 74 F g^{-1} and 88% coloumbic efficiency for 500 cycles at a high current of 500 mA/g. In addition to the excellent electrochemical properties of these activated carbons. The study performed opens new doors in the research for new carbon materials for EDLC applications due to the green processing, the cost associated with the precursor, and the simplicity in the activation process.[26].

In 2016, Zhou et al. obtained low-cost biomass-based carbon fibers from waste cotton linter with decent tensile strength reaching 0.72 GPa and the carbon yield up to 36.4%. They found that the carbon yield can be effectively improved by using dibasic ammonium phosphate as impregnant. Prepared CFs had a smooth surface, approximately circular and compact transverse texture in the cross-section. The obtained fibers show to be promising precursors for the preparation of quality CFs. The fibers exhibit a turbostratic structure.[27]

In 2016, Wang et al. researched the electrochemical properties of Platanus fruit-derived porous carbon. They synthesized the activated Platanus fruit carbon (a-PFC) by carbonization and alkali activation of PF. The as-prepared product demonstrated a highly porous network with a large fraction of micropores, high BET surface area and partial graphitization. It was showed a desired capacitive performance, including high specific capacitance, rate capability, and cycling stability when employed as electrode material for supercapacitor. The well capacitive performance manifests the vast potential of a PFC as energy and environmental materials.[28]

In 2018, Du et al. made research on Raw cotton-derived N-doped carbon fiber aerogel as an efficient electrode for electrochemical capacitors. They demonstrated a feasible and economic strategy for the scalable fabrication

of N-CFA. The raw cotton was employed as a fibrous template to fabricate shaped aerogels, and ZIF-8 (Zeolitic imidazolate framework, is a class of metal-organic frameworks) was in situ fabricated on the surface of cotton to create a rich porous structure and nitrogen doping. As a binder-free electrode, the N-CFA showed a remarkable capacity of 365 F g^{-1} at current 0.5 A g^{-1}. Additionally, the N-CFA exhibited an excellent rate capability. CFs obtained good stability with high capacitance retention of 93.6% after 10000 consecutive cycles at 5 A g^{-1}. They also anticipated using ZIF-8 modified raw cotton to fabricate shaped aerogels providing a new orientation for N-CFA preparation, which have broad applications in supercapacitors, lithium-ion batteries, sensors, and so on[29].

In 2018, Qiu et al. Prepared porous carbon materials to be electrode materials for supercapacitors by using corn straw biochar as precursor and KOH as activation agent. They highlight that prepared biochar-based carbon materials possess hierarchical micro-meso-macroporosity and very high specific surface areas. Due to multi-leveled pores' synergetic effect, the BBC-4 material shows excellent capacitive properties in the basic, acidic, and neutral electrolytes, such as high specific capacitance up to 327 F g^{-1}, high rate performance, and high work voltage. The carbon material also possesses excellent long-term stability up to 120 000 cycles and remarkable energy density. Proving that the biochar-based porous carbons are an auspicious electrode material for supercapacitors. More importantly, it opened up the new possibility of the utilization of biochar in high value-added areas.[30]

In 2018, Zhang et al. studied high-performance activated carbon fibers with a high micropore volume and large specific surface area using coconut fiber as a precursor via high-temperature carbonization KOH activation processes. It was found that the activation process could effectively increase the specific surface area of carbon materials by forming numerous micropores and inhibiting the formation and precipitation of tar on the surface of carbon fibers[31].

In 2019, Wu et al. Synthesized a new type of electrode material from natural products, cotton carbon fiber. The rationally designed AgNP/NCF sensing platform exhibited outstanding electro-catalytic activity to the superoxide anion. It offered a linear range of 10 orders of magnitude and a super low detection limit[32].

2.3   Carbon fibers

Carbon is one of the most abundant materials in nature and has been widely used in multiple applications for many decades. It is also noticeable that carbon has many allotropes with very different physicochemical properties. Depending on the particular application, one could choose between the following allotropes: coke, amorphous carbon, diamond, graphite, carbon nanotubes, carbon fibers, and others. Among those allotropes, (carbon fiber) CF is defined as a fiber-containing at least 92 wt % carbon, while the fiber-containing at least 99 wt % carbon is usually called a (graphite fiber) GF[33].

The fibers' size is an essential topic inside the use of carbon as a base for making any micro or nanodevice. A microfiber is an ideal form due to its mechanical properties, such as toughness, flexibility, and 2D-3D formability. That is the reason why CFs can be applied for creating textile structures like braids, wovens, and knits, as well as of continuous or chopped fibers[34]. It is also important to emphasize using (Carbon nanotubes fibers) CNTFs and (Graphene Fibers) GFs. When comparing them to solid CFs, they also show excellent mechanical properties, besides good electrical conductivity, light-weight, porous structure, and of course, the facility of being integrated with various guest nanomaterials. (A whole new world of devices can see the light with this). Also, CNTFs and GFs

have other unique properties inherited from CNTs and graphene, including large-surface areas and without forgetting physicochemical properties by chemical and heteroatom doping[35,36].

Besides PAN, different kinds of precursors produce carbon fibers, and depending on the precursor and the processing conditions, the fibers could gain specific properties. However, the essential features do not change and are still very similar.

Then, by far it has been mentioned the existence of multiple ways for obtaining CFs, the most common:

- Carbon fibers based on Poly(acrylonitrile) (PAN)

- Pitch-based carbon fibers

- Cellulose-based carbon fibers

- Lignin-based carbon fibers

- Poly(ethylene) (PE) based carbon fibers

- Other synthetic high-end precursors

Among the previously mentioned methods, cellulose and lignin are considered as very promising alternative precursors to PAN and mesoporous pitch because they are abundant in nature, and this means that they are relatively inexpensive and of course renewable[28,37–39]

CFs have shown to have promising properties for exploding in different areas, such as supercapacitors[30,40–44] or even they can be used as electrochemical sensors[45–47]. What makes them special is that they contain carbon atoms mostly; these fibers' diameter is about 5-10 micrometers. Moreover, carbon fibers have shown a diversity of properties, such that tensile properties, low densities, high thermal and chemical stabilities in the absence of oxidizing elements[33,48], and of course, excellent electric and thermal conductivities performance. Indeed, the first commercial production of carbon filaments is about 140 years ago, in 1879, according to Donnet[49], people applied it as an incandescent lamp filament. Besides, they made this filament from a cellulosic precursor. The carbon fiber's properties vary depending on the precursor.

In general, the final product's properties (CF or GF)s can be affected due to many factors such as the crystalline distribution, molecular orientation, the carbon content, and others[33]. Depending on the precursor selected for creating the fibers, CFs could be classified into Turbostratic of Graphitic, or even a mixture between them (a hybrid), where turbostratic and graphitic parts are present.

For Turbostratic, the sheets of carbon atoms are randomly folded, i.e., CFs derived from PAN. Moreover, for graphitic crystalline regions, the layer planes are stacked parallel to one another, just like we can appreciate in Fig.2.1. The atoms in a plane are bonded covalently through sp^2 bonding, and in the interaction between sheets, it is found relatively weak Van der Waals forces[33]. Additionally, the formation of conjugated sp^2 carbon atoms in the state during carbonization is beneficial for electrochemical applications. The ultimate performance of direct pyrolysis derived carbon (DPCs) in electrochemical applications is heavily reliant upon the structural and textural features, e.g., the porosity, morphology, and physicochemical properties, which are possibly designed by a judicious choice of organic precursors and the processing conditions (e.g., heating rate, residence time, and final temperature)[28].
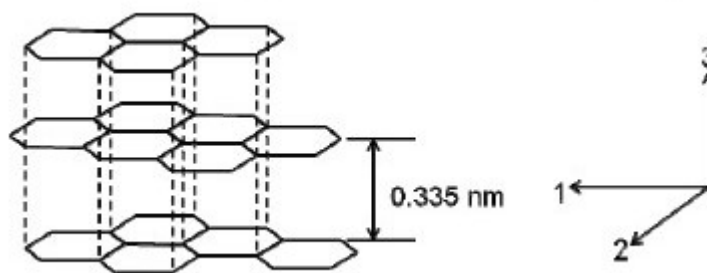
Figure 2.1: Structure of Graphitic crystals and crystal directions. Adapted from Singh et al, 2017[24]

The carbon fiber atomic structure is the same as graphite; this structure consists of carbon layers, which create a continuous hexagonal pattern. The communication among sheets is moderately powerless Van der Waals, molecules present in a plane are distributed in sp^2 holding[24].

2.4 Pyrolization

The CFs manufacturing process lies over-controlled pyrolysis of stabilized precursor fibers[50–53]. Usually, the heat treatment entails three steps: oxidization, carbonization, and graphitization[54].

The first step is to stabilize the precursor fibers by an oxidization process, for which it is necessary a temperature of about 200-400 °C in air. The next step is carbonization; here, it is needed to raise the temperature at around 1000 °C in an inert atmosphere to remove hydrogen, oxygen, nitrogen, and other non-carbon elements. Finally, CFs can be further graphitized when raising the temperature to around 3000 °C for achieving a higher carbon content and also a higher Young's modulus in the fiber direction[33].

Disordered carbons prepared by pyrolysis of organic precursors contain a predominantly planar hexagonal network of carbon atoms, but lack extended crystallographic ordering[4].

The performance of this biochar depends on the time of the reaction under a high-temperature condition.

In the literature, they mention that Physical activation is carried out at high temperatures (>700 °C) in the presence of gases like CO_2, H_2O, air, and ozone[1]. Yang et al. also describe that the process of physical activation has two steps: The first one, the carbonization process, which happens at a low temperature in an inert atmosphere, and during this process, volatile matters have been eliminated, and biochar is formed[1], what is happening is that the main components of biomass are being transferred into biochar through a series of reactions, such depolymerization, fragmentation, etc. Also, it should be noticeable that increasing the furnace's temperature and prolonging the treating time also help improve carbon materials' porosity. The pore size distribution will be broadened. However, biochars obtained through the method as mentioned above has low SSA and porosity, therefore for increasing SSA ofcarbon, the most common strategies includes physical and chemical activation[1].

For the present thesis, the activation of the carbon process will not be followed. Instead, it will be carried out a pyrolysis process under inert gas at two different temperatures for two different batches, the first one at 600 °C and

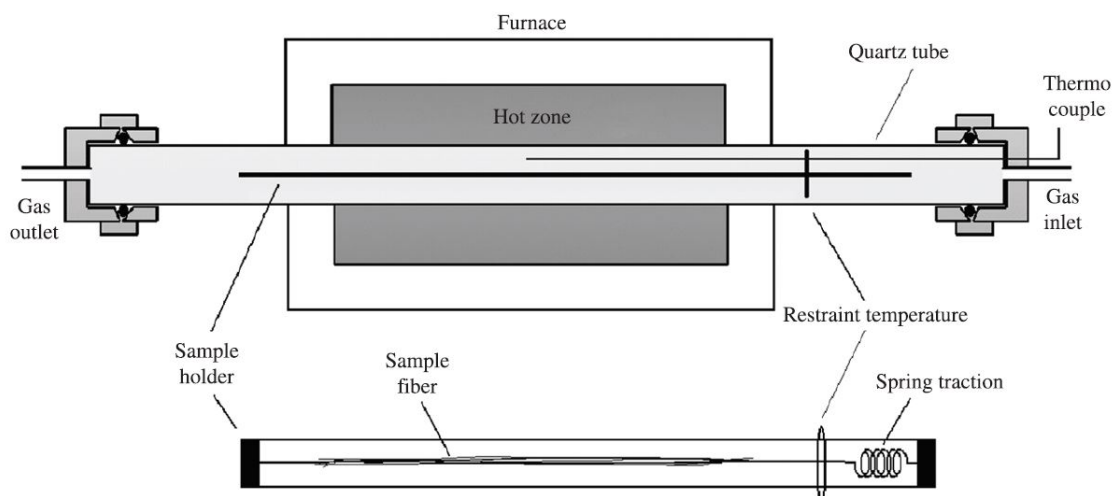the second batch at a maximum temperature of 1000 °C; the process is described in the following chapters.

Figure 2.2: Carbonization set up used to produce carbon fiber sample from oxidized textile PAN fiber. Adapted from Marcuzzo et al, 2017[55]

2.5 Functionalization

Functionalization is a chemical process that creates functional groups such as hydroxyl, carboxyl, nitrile, etc.

Those functional groups can facilitate the incorporation of other molecules for many applications. So an acidic agent is used for increasing the carboxyl (-COOH) and hydroxyl (-OH) groups to the surface. It is also capable of removing impurities from the amorphous carbon. On the negative side, with strong acid oxidation or a long time, carbon fibers' structure can be damaged, reducing their mechanical and electronic properties. Therefore, it is essential to stabilize a well-defined relationship between the functionalization parameters (acid concentration, time treatment) and the damage that a carbon fiber from biomass precursor can withstand without deteriorating its properties[56]. It has been observed that under the oxidation process, a variety of functional groups such as carboxylic (-COOH), carbonyl (-C = O), and hydroxyl (-OH) are formed on the surface of MWCNTs. These functional groups promote the chemical reactivity of MWCNTs[56,57]. Furthermore, we expect the same for CFs.

According to Zhang et al.[58], carbonous material surfaces, which must be chemically inert, manifest weak interfacial interactions, resulting in poor nanoparticle adhesion. Thus, the idea of functionalization is based on giving support for these materials by providing functional groups to which the Au, Ag, CeO_2, $CoFe_2O_4$, and Au/Fe_3O_4 nanoparticles adhere. Surface functionalization will be necessary to high deposition loadings of metal nanoparticles on the fibers because their surfaces are, as mentioned above, inert.

2.6 Electrochemistry and Electrochemical sensors

Electrochemistry, or electroanalytical chemistry, is defined as the branch of chemistry that examines the resultant phenomena from the combination of chemical and electrical effects. The controlled flow of electrons allows us to enjoy the beauty of technology: cellphones, laptops, cars, and others. Batteries are nothing but the resultant product of applied chemistry, specifically redox reactions playing a crucial role while rapidly meeting the changing scientific and research demands[59]. This flow of electrons between two atoms in a reduction-oxidation reaction produces electricity, which is later studied through different analysis types. One of the most exciting features of working in electrochemistry is that it depends on a surface phenomenon, not an optical path length. Therefore sample volumes can be tiny, lending themselves to miniaturization. Moreover, that is the importance of working with carbon fibers of about 5-10 mm long.

People probably do not think about electrochemical sensors often, but what is true is that these kinds of sensors can save lives. The development of electrochemical sensors has been of great interest over the last decade. The main reasons converge to the low-cost and sensitivity (indicated by low detection limits) of electrochemical transducers for detecting a variety of biological analytes[60,61]. Some researchers guarantee the use of electrochemical sensors because of their stability, reliability and because of their requirement of very little power for providing good results[62–64]. Modern electrochemical sensors are present in our daily lives, detecting several parameters, whether physical, chemical, or biological[3]. Some examples of electrochemical sensors' applications are sensors related to machines, sensors used in automobiles, environmental monitoring, and technology in general. The main objective of a chemical sensor is to provide reliable information in real-time, for instance, the chemical composition of its surrounding environment. Ideally, the final device will not perturb the sample[7].

2.6.1 Voltammetry

The needment for analytical sensors for knowing the quality of food, air, pharmaceutical, and chemical compounds are the reasons why electrochemical sensors have become an essential tool for researchers and, of course, inside industry[65,66]. In this way, to understand whats beyond an electrochemical sensor work, we shall start by dividing it into two general categories:

1. Potentiometric Sensors: In this case, the change in potential of the sensor occurs depending on the concentration of the analyte[67,68].

2. Voltammetric and amperometric sensors: In this case, oxidation-reduction reactions take place, creating a current that is dependent on the concentration of electroactive analyte[69,70]. In other words, the current is linearly proportional to the gas concentration.

One of the main differences between the Potentiometric and Amperometric sensors is that the first one work with a constant applied voltage and the sensor signal is given by a current, whilst the second one operates at zero current, and the sensor signal is the potential difference between the sensing electrode and a reference electrode[65].

Potentiometric sensors are desirable for field operations because of their high selectivity, simplicity, and low cost. However, they are less sensitive than their Voltammetric counterparts, so there is an increasing amount of research related to amperometric sensors. Besides, there are also sensors based on simple conductivity changes of ions. Also, a larger group of sensors are based on resistivity and impedance, such as capacitive sensors.

2.7   Fundamentals of Characterization Techniques

2.7.1   Synthesis of Nanoparticles

Nanoparticles can be synthesized by different methods that are categorized into bottom-up or top-down methods (See Figure 2.3).
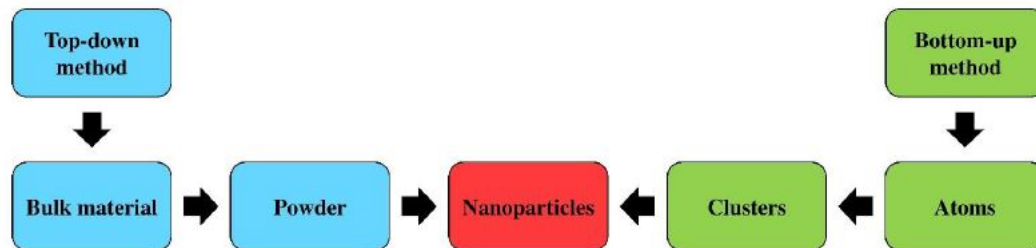
Figure 2.3: Synthesis Process. Adapted from Ealia et al[21], 2017.

Bottom-up method

The bottom-up method is a constructive method based on the build-up of material from atoms to clusters to nanoparticles.

The main commonly methods for nanoparticle production inside this branch:

- Sol-gel

- Spinning

- Chemical Vapour Deposition (CVD)

- Pyrolysis

- Biosynthesis

From the list above, the most important methods:

Sol-gel. The sol - a colloidal solution of solids suspended in a liquid phase. The gel - a solid macro-molecule submerged in a solvent. The Sol-Gel method represents the chemical transformation from a liquid into a gelatinous

network phase with subsequent post-treatment and transition into solid oxide material. The sol-gel process allows the synthesis of ceramic materials of high purity and homogeneity through preparation techniques different from the traditional method of fusion oxides. The main benefits of this process rely on the high purity and uniform nanostructures achieved at low temperatures. It is the most used method inside this branch because of its simplicity.[71]

Chemical vapor deposition (CVD) is a technique in which substances in the vapor phase are condensed to generate solid phase material. This method is helpful for produce high-quality, high-performance, solid materials, typically under vacuum. CVD is utilized to produce composite material films, CVD involves chemical reactions that takes place between an organometallic or halide compounds to be deposited and the other gases to produce nonvolatile solid thin films on substrates and infiltrating fabric in the production of different nanomaterials. This method changes optical, electrical, and mechanical attributes as well as the corrosion resistance of different substances.

The deposition occurs in a vacuum chamber by combining gas molecules. When a substrate is heated, a chemical reaction occurs when it comes in contact with the mixed gas. This chemical reaction produces a thin film of product on the substrate surface that is recovered and used. The surface is driven due to thermal energy, and the reaction process occurs in the presence of gas with an inert atmosphere.

The advantages of CVD are uniform, highly pure, complex, and strong nanoparticles. The disadvantages of CVD are the requirement of special equipment, and the gaseous by-products are highly toxic[21,72,73]

Bottom-down method

The bottom-down method is a "destructive" method based on the reduction of bulk material to nanometric scale particles. The most widely used NPs synthesis inside this branch:

- Mechanical Milling

- Nanolithography

- Laser Ablation

- Sputtering

- Thermal Decomposition

Sputtering technique is about the deposition of nanoparticles on a surface by ejecting particles from it by colliding with ions. Usually, sputtering deposition deal with placing a thin layer of nanoparticles followed by annealing. The shape and size of the nanoparticles are dependent on the thickness of the layer as well as the temperature and duration of annealing[21].

Thermal decomposition is a technique where the nanoparticles are produced by decomposing the metal at specific temperatures undergoing a chemical reaction producing secondary products. Thermal decomposition is an endothermic chemical decomposition where temperature and heat are responsible for breaking the chemical bonds of the compound[21]

2.7.2   Scanning Electron Microscopy

The SEM uses an electron beam to create detailed images of its specimen.

A scanning beam of electrons is directed at the sample within a vacuum. As the electrons hit the sample, they scatter. This scattering of electrons is used to generate a detailed image of the sample fiber. Since the SEM uses electrons in its imaging process, the specimen must be conductive, or it will begin to charge. Charging interferes with the imaging process, causing the sample image to blur.

SEM can provide information on surface topography besides of the crystalline structure, chemical composition, and electrical behavior of the top 1 μmeter or so of specimen[74]. Various specialized stages (e.g., hot, cold, or designed to permit in situ mechanical testing) can be attached to enable behavior under different conditions to be examined. For example, cathodoluminescence (emission of light) at temperatures near absolute zero is much stronger than at room temperature, so images formed from the light emitted by a cold specimen are much less noisy[74].

Further advantages of SEM include: SEM benefits from a large depth of field, so most of the specimen surface is simultaneously focused on surface roughness. Much higher magnifications can be achieved (up to 1,000,000x), with an ultimate resolution of 1 nm.

Moreover, the images obtained in this work were obtained with the Backscatter electron detector (BSD) inside the SEM. Backscattered electrons are those incident electrons that approach an atom's nucleus sufficiently closely to be scattered through a large angle and reemerge from the surface. Even if they are not as numerous as secondary electrons, they have much higher energies. Images have slightly less resolution than secondary electron images because they come from deeper zones in the specimen, so the area giving rise to the signal is larger than the probe size. In here is important to mention that BSE provide compositional information: elements of higher atomic mass give brighter contrast[74].
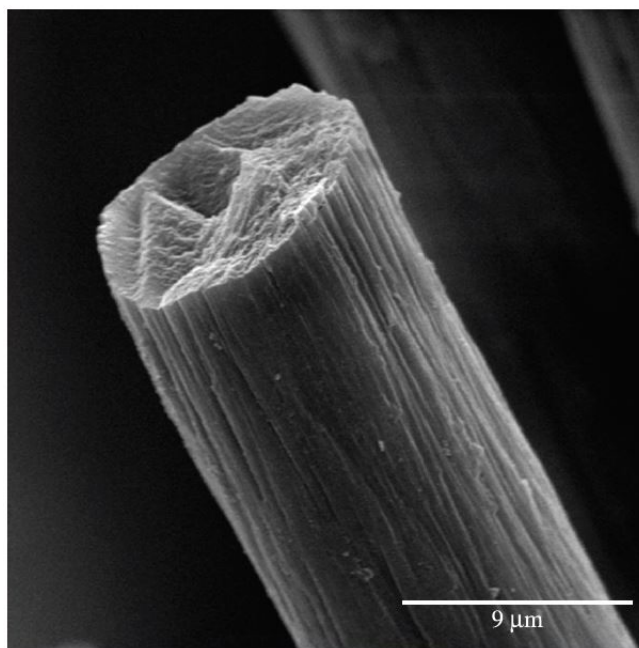
Figure 2.4: SEM micrograph of commercial oxidized Pan fiber (PANOX®). Adapted from Marcuzzo et al, 2017[55]

2.7.3 RAMAN

Raman Spectroscopy is a high-resolution photonic technique that provides chemical and structural information in just a few seconds of almost any organic or inorganic material or compound, thus allowing its identification. The analysis employing Raman spectroscopy is based on examining the light scattered by a material when incident on it a monochromatic beam of light. A small portion of the light is inelastically scattered, undergoing slight frequency changes characteristic of the analyzed material and independent of the incident light frequency. It is an analysis technique that is carried out directly on the material to be analyzed without any special preparation. That does not entail any alteration of the surface on which the analysis is carried out. That is, it is non-destructive[75].

In carbonous samples, two bands are recognized just like a fingerprint; those are the D and G bands, whose information is of great importance in studying structural defects of the CFs. The graphitic G peak is attributed to the bond stretching of all sp^2 atoms in chains and rings; while, the D peak corresponds to the breathing mode of sp^2 atoms in rings characteristic of disorder defect within the carbon matrix. The (I_D/I_G) values are determined to determine further the formation of defects in the different fibers prepared[30,50,58].

The intensity ratio of the D band with respect to the G band (I_D/I_G), also known as the Tuinstra-Koenig relation, has been used widely to analyze the Raman spectra of carbon materials and could still apply to the carbon fibers even though they are the mixtures of sp^2 carbon layers and sp^2 carbon clusters[76] The ratio I_D/I_G ratio is widely used to describe the structural purity and defect quantity of graphitic material and can provide an understanding of the

crystallinity of the fibre[77,78]. Only the D and G bands were observed in the Raman spectra of the two batches of this work.
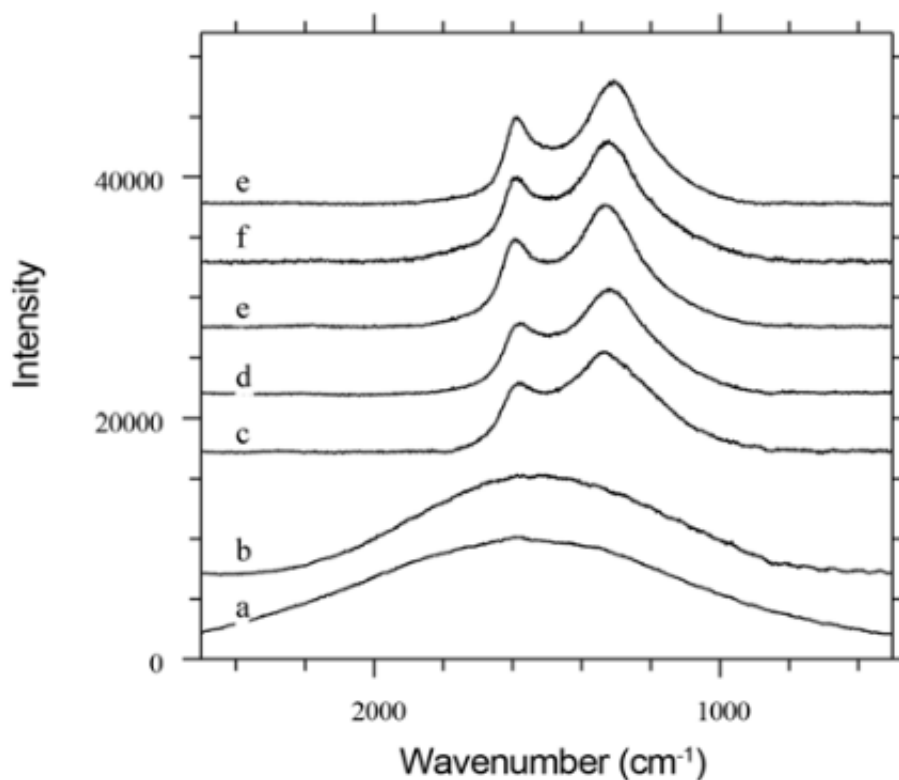

Figure 2.5: Raman spectra of carbon fibers prepared at (a) 500 °C, (b) 600 °C, (c) 700 °C, (d) 800 °C, (e) 900 °C, (f) 1000 °C, and (g) 1100 °C. Adapted from Karacan et al, 2018[79]

Figure 2.5 shows the typical Raman spectra of the carbon fibers prepared in the temperature range between 500 and 1100 °C[79], the change in temperature affects the raman shift of the band, as well as, the narrowing of them.

2.7.4   XPS

X-ray photoelectron spectroscopy (XPS) is a non-destructive and ultra-high vacuum characterization technique used for crystalline materials. XPS is helpful for quantitative analysis of surface composition and can detect all elements except for hydrogen and helium by detecting the binding energies of the photoelectrons. Besides provides information on structures, phases, crystal orientations (texture), and other proper parameters, such as crystallinity and crystal defects. Inside the XPS, peaks are constructed due to the constructive interference of a monochromatic beam of X-rays scattered at specific angles from each set of lattice planes in the sample. To identify chemical states, small

variations in binding energies of the photoelectron lines and Auger lines, as well as, satellite peaks, and multiple splitting can be used. XPS is initiated by irradiating a sample with monoenergetic soft X-rays, most commonly Mg Kα (1253.6 eV with a line width $\approx$ 0.7 eV) or Al Kα (1486.6 eV with a line width $\approx$ 0.85 eV). In many modern instruments the Al Kα X-ray line is further narrowed (to $\approx$ 0.35 eV) using a monchrometer[80–82].
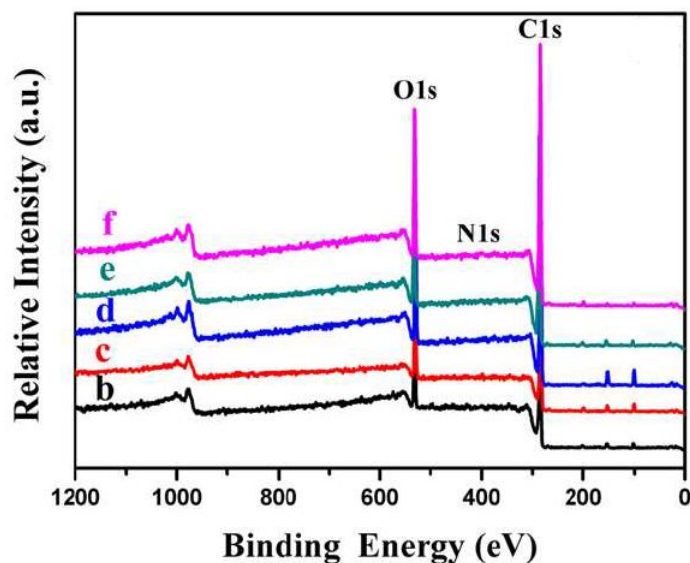

Figure 2.6: XPS spectra of waste carbon fiber. Adapted from Nie et al, 2015[83]

2.7.5   Fourier Transform Infrared (FTIR) spectroscopy

FTIR is an analytical methodology used in industry and academic laboratories to understand individual molecules' structure and molecular mixtures' composition. This type of spectroscopy uses modulated, mid-infrared energy to study a sample. Depending on the material, the infrared light is absorbed in specific frequencies related to the functional groups' vibrational bond energies present in the molecule. A characteristic pattern is formed, which is the vibrational spectrum of the molecule. These spectral bands' position and intensity provide a fingerprint of molecular structure, making FTIR spectroscopy a highly adaptable and useful technique. FTIR spectroscopy is a significant advance over the traditional dispersive infrared approach for many reasons, including that the entire FTIR spectrum is collected in a fraction of second and co-adding spectra, signal-to-noise is improved[84].

The IR spectrum obtained from the FTIR spectrometer lies in the mid-IR region between 4000 and 600 cm^{-1}. Over the X-axis, the spectra describe the infrared radiation in wavelength's unit cm^{-1}, and the Y-axis shows the intensity of infrared radiation absorbed. The spectra are composed of a series of absorption peaks positioned at different positions, heights, and widths. In the mid-IR region (4000-400 cm^{-1}) are located the transition energies corresponding to changes in vibrational energy state for many functional groups. Thus the absorption band in this

region can be used to determine if any specific functional group exist within the molecule.

Typically, there are four regions of types of bonds that can be analyzed from the FTIR spectra. As shown in Fig. 2.7, a single bond (O-H, C-H, and N-H) is detectable in higher wavenumber (4000-2500 cm^{-1}). Besides, the triple bond and double bond are observable in the middle wavenumber region 2500-2000 cm^{-1} and 2000-1500 cm^{-1}, respectively. Additionally, the region between 1500-500 cm^{-1}, also called the fingerprint region, is generated due to different bond vibrations present on the structure (skeleton) of the molecules, which is unique of each molecule or group of molecules[85,86].
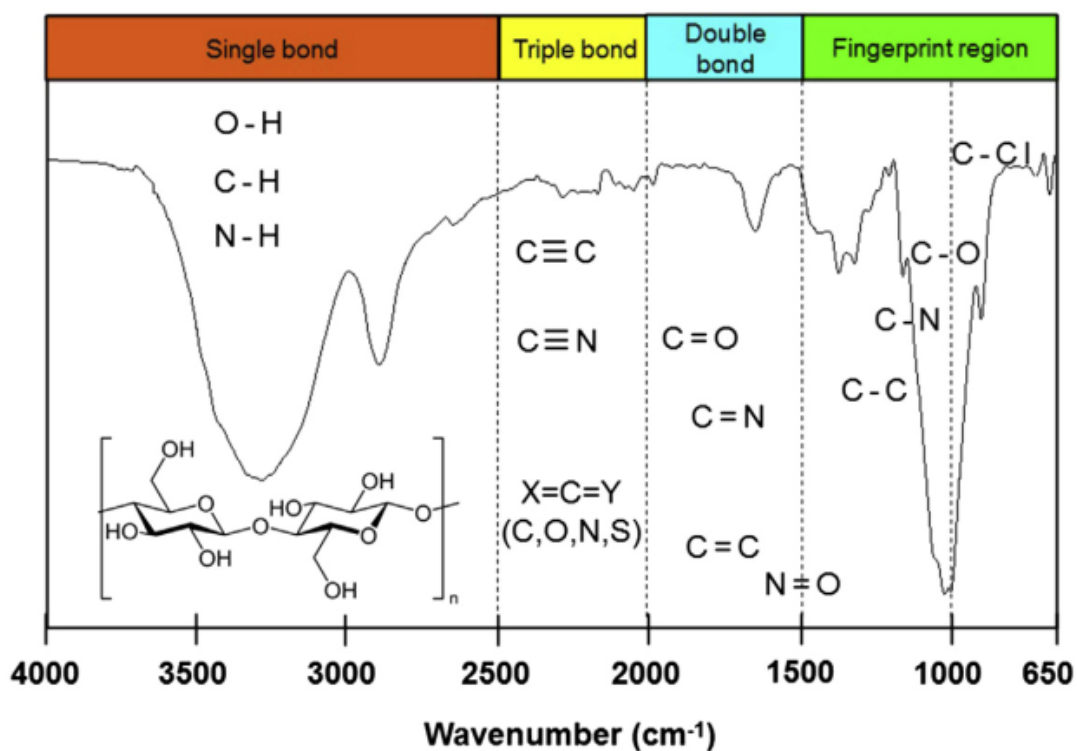

Figure 2.7: Typical Fourier transform infrared spectra of regenerated cellulose membrane with the various common types of bonds absorb in the approximate regions. Inset correspond to cellulose molecular structure. Adapted from Mohamed et al[86], 2017.

2.7.6   Cyclic voltammetry

Cyclic voltammetry (CV) is a well-known and influential electrochemical technique employed to investigate the redox (reduction and oxidation) molecular species processes.

Cyclic voltammetry uses a triangular potential waveform initially. Chemical species that are undergoing oxidation

or reduction at the electrode surface is seen when a potencial scans linearly over time, and when the potential reaches a sufficiently negative/positive potential, yielding an electrical current. The number of chemical species which are undergoing a redox process per unit time can be quantified thanks to this current.

When the electrode potential is scanned in a positive direction, an oxidation reaction is occuring at the electrode surface and it can be observed an oxidative (or anodic) current starting at the onset potential of the redox event (where the background-subtracted current becomes non-zero). As the potential increases through the redox-active species' half-wave potential (E 1/2), oxidation becomes more thermodynamically favorable, and hence the current extends until the oxidation phase is finally confined by species diffusion to the electrode surface, resulting in a diffusional tail characterized by a decrease in the current.

After that, the electrode's potential sweep is reversed and scanned in the opposite direction before it hits the initial potential. The reduction of the electrochemically produced species results in a cathodic (reductive) current in a chemically reversible electron-transfer process (denoted an E mechanism). By changing the scan rate (the rate at which the potential is scanned) and keeping track of the differences in the current response, valuable kinetic parameters can be obtained. During the potential scan of CV, the concentrations of redox-active species at the electrode interface change over time by undergoing electron transfer to reach the equilibrium position as defined by the Nernst equation 2.1, which results in the observed change in the current response.[87]

In potentiometric sensors, the analytical information is obtained thanks to the well known Nernst equation which logarithmically relates the measured electrode potential, E, to the relative activities of the redox species of interest:

$$E = E^0 + \frac{RT}{nF} ln \frac{a^0}{a^R} \tag{2.1}$$

In eq.2.1. E^0 represent the standard electrode potential, a^0 and a^R are the respective activities of the oxidized and reduced species, R represents the universal gas constant, T is the absolute temperature, F is the Faraday constant and n is the number of moles of electrons exchanged in the electrochemical reaction.

The principle on which electrochemical sensors operate takes place on an electrical current passing through a sensing electrode produced by an electrochemical reaction. For instance, inside of an Amperometric sensor, we can find a sensing electrode, a counter electrode, an electrolyte, and usually a reference electrode. Once outer particles reach the sensor, what is happening inside is a redox reaction that produces or consumes electrons and generates an electric current (signal).

Voltammetry provides an electroanalytical method implying a varying voltage where the current is linearly dependent upon the analyte concentration involved in a chemical or biological recognition process (at a scanned or fixed potential).

Cyclic voltammetry profile

In the Voltammograms or cyclic voltammograms, the CV will describe two axes.The x axis represents a parameter which the user imposes to the system, this is so-called **the applied potential** E [V], meanwhile the y axis is **the response** (resulting current [A]) to the applied potential.

There is another important parameter that one must take into account. This parameter is the so-called **Scan Rate**. The scan rate indicates the variation of the potential concerning time, i.e., $100[mV/s]$.
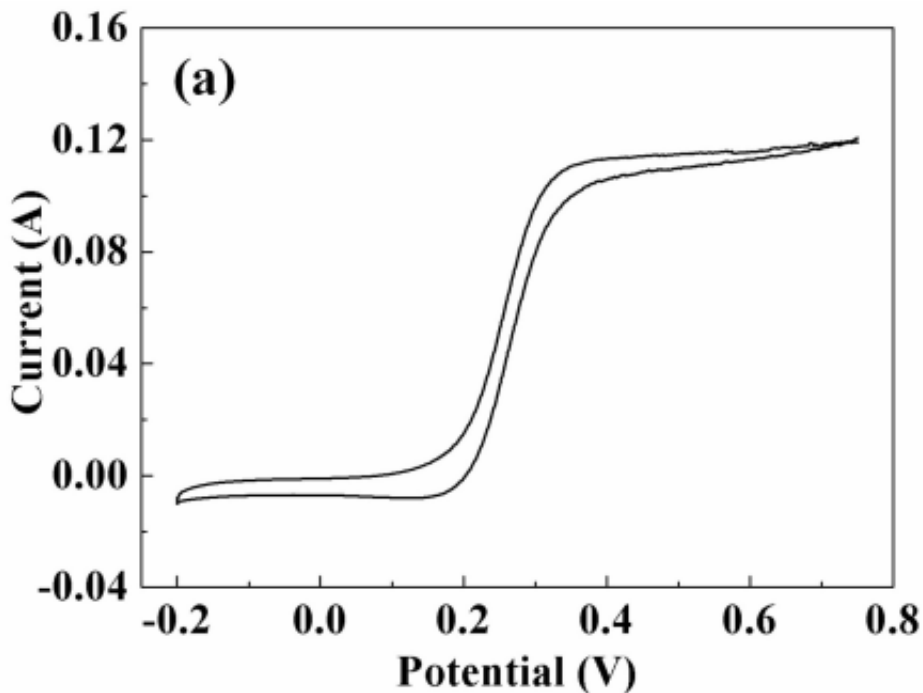

Figure 2.8: CV of PAN-based CF adapted from Elgrishi et al, 2017[88].

Figure 2.8 shows the CV curves of the a carbon fiber micro-electrode in 5.0 mM K 4 Fe(CN) 6 , performed at a scan rate of 0.10 V·s^{-1} . As shown, the CV of PAN-based CF exhibits a highly symmetrical shape for both the forward and reverse potential scans, indicating that highly reversible redox reactions are taking place at the carbon fiber. It demonstrates that the carbon fiber, as microelectrode, exhibit an outstanding electrochemical property in the presence of $K_4Fe(CN)_6$ [88].

Chapter 3

Experimental

3.1 Methology

3.1.1 Recollection

In this work, two samples of banana trees were used. **The first banana trunk** was collected from Urcuqui-Ibarra, located in the province of Imbabura-Ecuador, **the second trunk** was collected in the province of Santo Domingo "Las Mercedes."

These trees, belong to the family *Musaceae* and genus Musa, specie *Musa Paradisíaca*. The first tree sample was too young, and the pseudo-stem (the trunk's heart) was different from the second one. The first sample's pseudo-stem had about 20mm of radius and did not present any fruit.

The sample of the second tree comes from a plant whose fruit had previously been harvested. It consisted of a 30 cm^{-1} trunk weighing approximately 2kg (See Figure 3.1). The pseudo-stem had a radius of about 35 mm of the radius.

Figure 3.1: *Musa Paradisíaca*.

Once it was obtained the pseudo-stem (after removing the protection layers), the fibers were obtained using a scalpel and performing a cut over the profile of the cylinder carefully, and then by applying force, the pseudo-stem was broken and stretched, the final result is a magnificent batch of fibers which can be seen in Fig 3.2.

Figure 3.2: Obtaining of raw fibers.

3.1.2 Pyrolyzation

To pyrolyze biomass material (pseudo-stem banana fibers in this work), it is needed to design a system to keep the samples anchored and avoid them from falling into the furnace and creating a mess.

So, the design was carried out in the Physical Sciences and Nanotechnology school's mechanical workshop property and can be appreciated in Figure 3.3.

Also, it is essential to mention that the pyrolysis process was carried out under an inert atmosphere with an Argon flux of 0.30 mL per minute. This configuration was programmed in the tubular furnace (see Fig. 3.17).

It was Pyrolyzed a **total of two batches of fibers**, and the procedure is described below.

Figure 3.3: Spike mounting for pyrolizing fibers inside the tubular furnace.

Batch one

The first batch of fibers belongs to the first sample of banana stem collected in Urcuqui, as mentioned above. Moreover, the mounting of fibers can be seen in Figure 3.4.

Figure 3.4: Sample of fibers anchored to the assembly.

For the first batch of fibers, it was worked (pyrolyzed) at a maximum temperature of 600 °C, with a heating ramp denoted in Table 3.1 and can be seen in figure 3.5.

Heating ramp	
Time [min]	**Temperature [°C]**
0 - 10	100
10 - 40	200
40 - 70	300
70 - 100	400
100 - 130	500
130 - 160	600

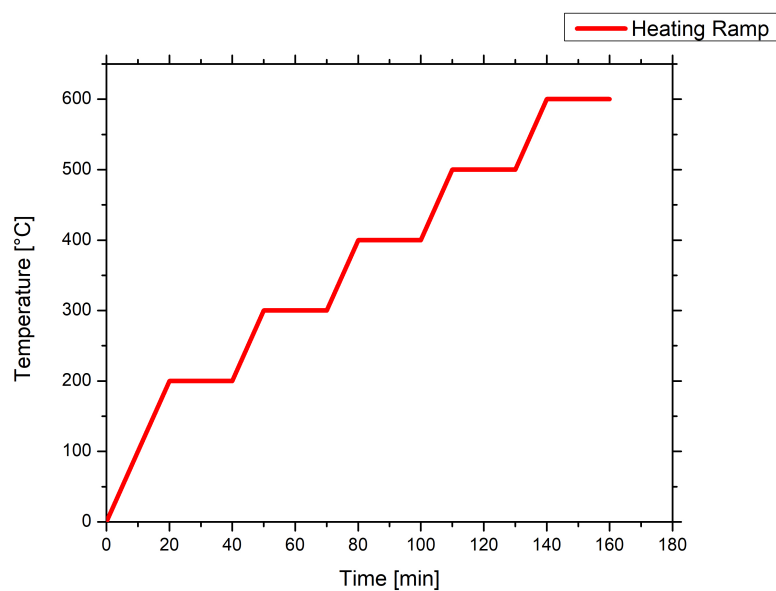Table 3.1: Heating ramp for the first batch of fibers.

Figure 3.5: Heating ramp for the first batch of fibers.

The final product after pyrolysis into the tubular furnace can be seen in Figure 3.6

Figure 3.6: Pyrolyzed fibers of batch one.

Batch 2

Before taking the fibers into the pyrolysis process, they were previously dried into the oven at 65 °C all night long (See Figure 3.7.). This prevents the fibers from rotting due to the high content of water and sugars and, of course, do

not lose our main character of the study.

Figure 3.7: LHS: Fibers left into the oven at 65 °C. RHS: Dried fibers ready to pyrolize.

The second batch of fibers was worked (Pyrolyzed) at a maximum temperature of 1000 °C, with a heating ramp denoted in Table 3.2 and can be appreaciated in Figure 3.8.

Heating ramp	
Time [min]	**Temperature [°C]**
0 - 10	200
10 - 20	400
20 - 30	600
30 - 40	800
40 - 50	1000
50 - 60	1000

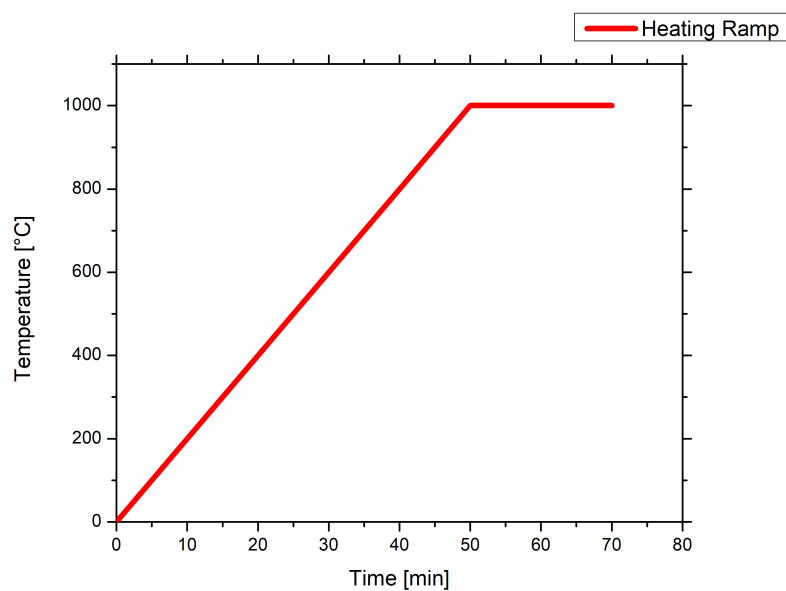Table 3.2: Heating ramp for the second and third batch of fibers.

Figure 3.8: Heating ramp for the second and third batch of fibers.

The final product after pyrolysis into the tubular furnace can be seen in Figure 3.9.
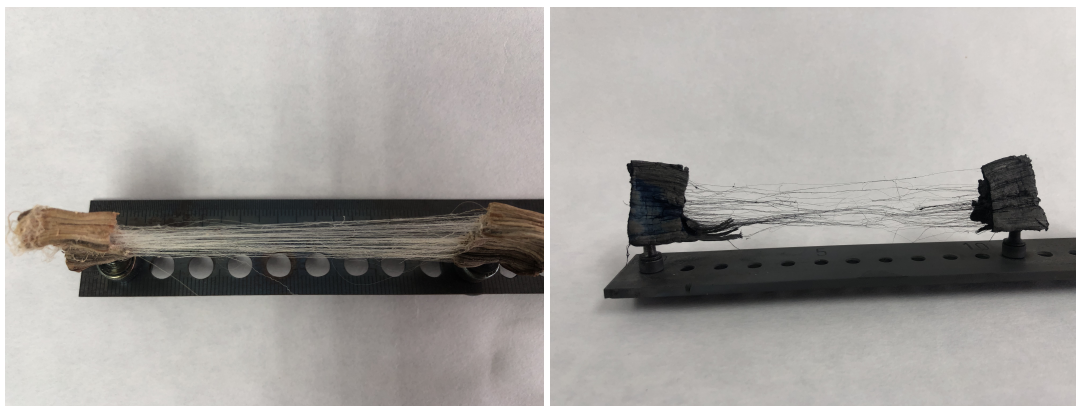

Figure 3.9: LHS: Dry fiber before pyrolysis process. RHS: Pyrolyzed fiber.

3.1.3 Functionalization

It is necessary to clarify that **only the fibers of batch two** were taken to functionalization.

Prefunctionalization and functionalization step is central to add functional groups to the fiber surface, the carbon fibers are taken to an acidic treatment, and the methodology is listed below:

Prefunctionalization

Prefunctionalization		
Chemical	**Volume [mL]**	**Molarity [mmol]**
Nitric acid	100	3
Sulfuric acid	300	1

Table 3.3: Pre-functionalization acids

The Pyrolyzed carbon fibers were introduced into a 500[mL] volumetric flask, then the nitric and sulfuric acids were added softly. The volumetric flask with the reaction mixture was put under reflux at a temperature of 80 ° C for 35 minutes (See Fig. 3.10). Once the time was over, the mixture is allowed to cool at room temperature, and the fibers were washed, adding deionized water several times.

Figure 3.10: Prefunctionalization process.

Functionalization

Functionalization		
Chemical	**Volume [mL]**	**Molarity [mmol]**
Nitric acid	100	65

Table 3.4: Functionalization treatment

The carbon fibers pre-functionalized obtained before were placed into a 250 mL volumetric flask, and then the nitric acid was added softly. The volumetric flask with the reaction mixture was under reflux at a temperature of 80 °C for 60 minutes, and after the time was over, the mixture is allowed to cool at room temperature, and the fibers were washed, adding deionized water. Finally, the fibers were left in the oven at 65 °C per 30 min (until they were completely dried).

3.1.4 Synthesis of Nanoparticles

To decorate the fibers, the nanoparticles employed were synthesized, and CeO_2 nanoparticles were of commercial origin. Therefore, it was needed to synthesize Au, Ag, $CoFe_2O_4$ and Au/Fe_3O_4 nanoparticles with the methodology described below.

Synthesis of Au nanoparticles

0.83 g (2.2 mmol) of chloroauric acid ($HAuCl_4$), 3.1 g (1.2 mmol) of 1,2-hexadecanediol, 0.5 mL (1.5 mmol) of oleic acid and 3 mL (6 mmol) of oleylamine were added into 30 mL of phenyl ether. Under argon atmosphere and vigorous stirring, the reaction solution was heated to 180-190 °C at 10 °C/min and was kept at this temperature for 1.5 h. After cooling to room temperature, ethanol was added to the solution. A dark-purple material was precipitated and separated by centrifugation. The precipitated product was washed with ethanol and redispersed in 0.1 g of CTAB in 100 mL of distilled water.

Synthesis of AuFe$_3$O$_4$/CTAB nanoparticles

The experimental setup consisted of a system reflux under N_2 atmosphere using a 250 mL condenser and heating mantle. The procedure consisted of mixing Fe(acac)$_3$ (2 mmol), 1,2-hexadecanediol (10 mmol), oleic acid (6 mmol), oleylamine (6 mmol), and benzyl alcohol (20 mL). The nuclei formation and the growth were obtained when the temperature was increased for 200 °C for 30 min under partial vacuum and then, under a blanket of argon, heated to reflux 265 °C for another 30 min. The black-brown mixture was cooled to room temperature by removing the heat source. Under ambient conditions, ethanol (40 mL) was added to the mixture, and a black material was precipitated and separated via centrifugation. The product was dissolved in hexane in the presence of oleic acid (0.05 mL) and oleylamine (0.05 mL).

10 mL of the phenyl ether reaction solution of Fe_3O_4 nanoparticles (0.33 mmol Fe_3O_4), 0.83 g (2.2 mmol) of Chloroauric acid ($HAuCl_4$), 3.1 g (12 mmol) of 1,2-hexadecanediol, 0.5 mL (1.5 mmol) of oleic acid and 3 mL (6 mmol) of oleylamine were added into 30 mL of phenyl ether. In this case, the mole ratio of the Au precursor to the iron oxide nanoparticles was approximately 7:1. Under argon atmosphere and vigorous stirring, the reaction solution was heated to 180-190 °C at 10 °C/min and was kept at this temperature for 1.5 h. After cooling to room temperature, ethanol was added to the solution. A dark-purple material was precipitated and separated by centrifuging. The precipitated product was washed with ethanol and redispersed in hexane in the presence of 75 mmol each of oleic acid and oleylamine. The nanoparticle solution appeared dark purple. The product nanoparticles dispersed in hexane, which can be further separated by centrifugation to obtain the desired core-shell Fe_3O_4/Au nanoparticles. The Au-coated Fe_3O_4 nanoparticles are then transferred into water by mixing them with sodium citrate and cetyltrimethylammonium bromide (CTAB).

Synthesis of $CoFe_2O_4$ nanoparticles

Co(acac)$_3$ (1 mmol), Fe(acac)$_3$ (2 mmol), 1,2-hexadecanediol (10 mmol), oleic acid (6 mmol), oleylamine (6 mmol) and phenyl ether (20 mL) were mixed and magnetically stirred. The mixture was heated to 200 °C for 30 min and then, heated to reflux (265 °C) for another 30 min. The black-brown mixture was cooled to room temperature by removing the heat source. Ethanol (40 mL) was added to the mixture under ambient conditions, and a black material was precipitated and separated via centrifugation.

Synthesis of Ag nanoparticles

28.474 mL of demineralized water was put into a 50 mL beaker. Then, 150 mL of AgNO3 (0.05 M) and 400 mL of TSC (75 mmol) were added and vigorously stirred for 3 min. Then, 4 mL of $NaBH_4$ (100 mmol) was rapidly added, leading to a light yellow solution. After 2 min of stirring, 60 mL of H_2O_2 (30 wt%) were added, converting the yellowish solution to a colorless one. Finally, 250 mL of $NaBH_4$ (100 mmol) was rapidly injected, leading to a fast change in colors that ended up in reddish-yellow.

3.1.5 Decorating with Nanoparticles

Batch One

Before the pyrolyzation process, batch one was decorated in situ with the nanoparticles by immersion method, which consisted of introducing them into a nanoparticles bath for 18 hours. (See Fig. 3.11). And then, finally, they were taken into the tubular furnace for the respective pyrolysis process.

Li et al., reported a Co nanoparticles supported on cotton-based carbon fibers, where the cotton was first immersed in an aqueous solution of NPs for 24 h, then the fibers were dried at 60 °C and immediately pyrolyzed to 600 °C and 700 °C at a heating rate of 4 °C/min in N_2 atmosphere and annealed for 2 h[89].

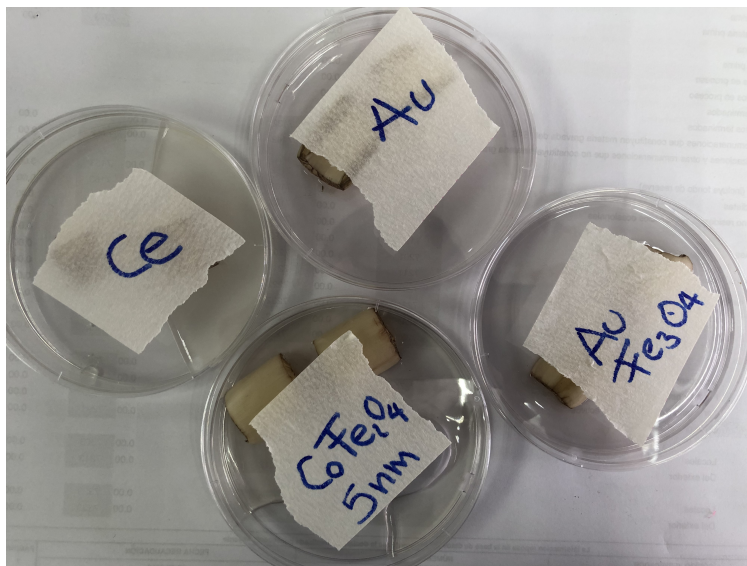In contrast, the nanoparticles applied in this process can be seen in figure 3.12.

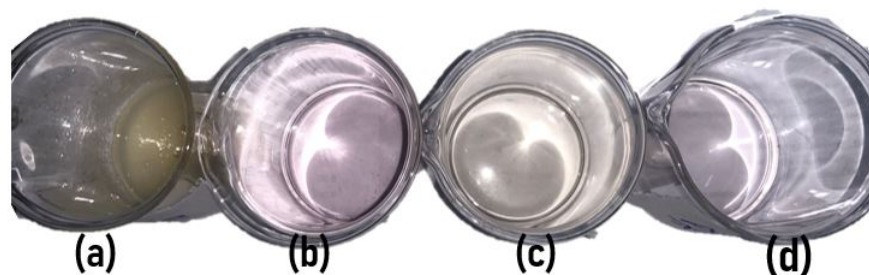Figure 3.11: Raw fibers decorated with NPs.

Figure 3.12: (a) Ceria NPs, (b) Gold NPs, (c) CoFe$_2$O$_4$, (d) AuFe$_3$O$_4$ nanoparticles

Batch Two

The fibers were first pyrolyzed for the second batch, then functionalized, adding carboxyl (-COOH) and hydroxyl (-OH) groups over the surface.

Thanks to this process, it was expected to obtain a larger quantity of nanoparticles stuck to the CFs surface. The nanoparticles applied in this process can also be seen in figure 3.14.

Pyrolyzed carbon fibers were decorated in situ, putting the fibers in immersion and then left drying into the oven for 24 hours at 65 °C. The next step was to prepare the fibers for the different characterization techniques.
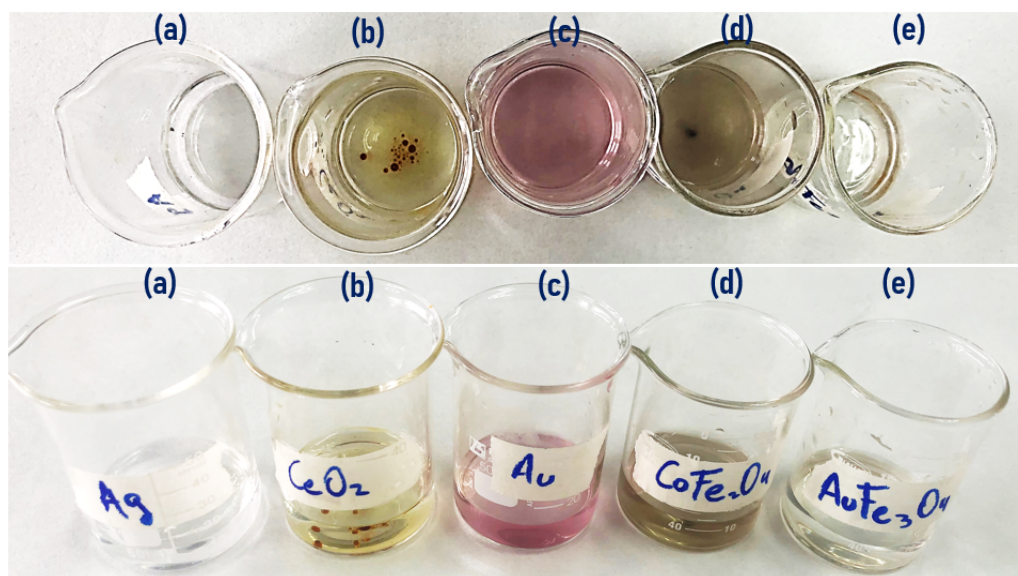
Figure 3.13: (a) Ag NPs, (b) CeO$_2$ NPs, (c) Au, (d) CoFe$_2$O$_4$, (e) AuFe$_3$O$_4$ nanoparticles.
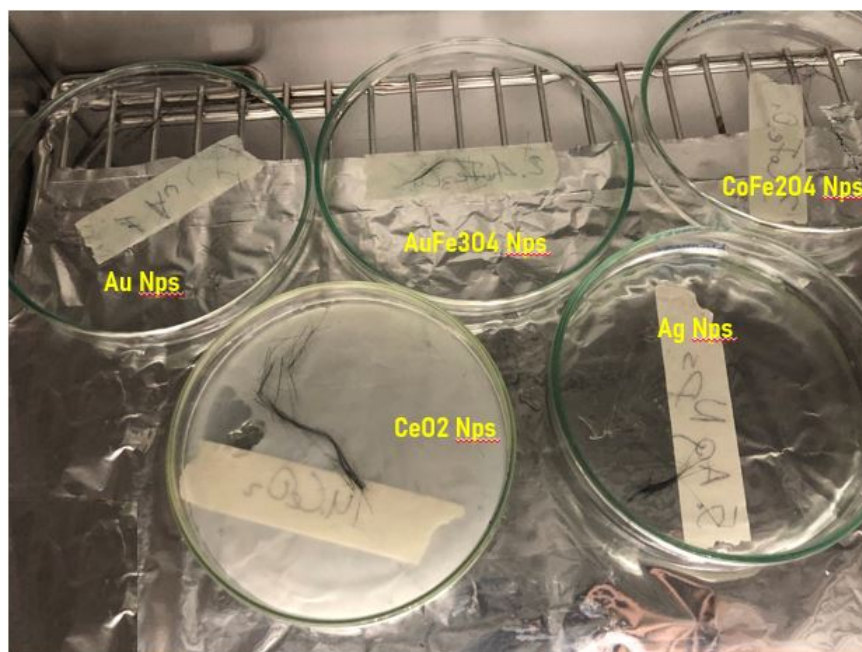

Figure 3.14: Functionalized fibers decorated with nanoparticles drying into the oven.

3.1.6   Electrodes

The electrodes were created by hand (figure 3.16), following the scheme used by (Lu, et al,2017)[45] which can be seen in Fig.3.15 A segment of carbon fibers of about 1 cm^{-1} was attached to the electrode, by pasting it with silver paint.
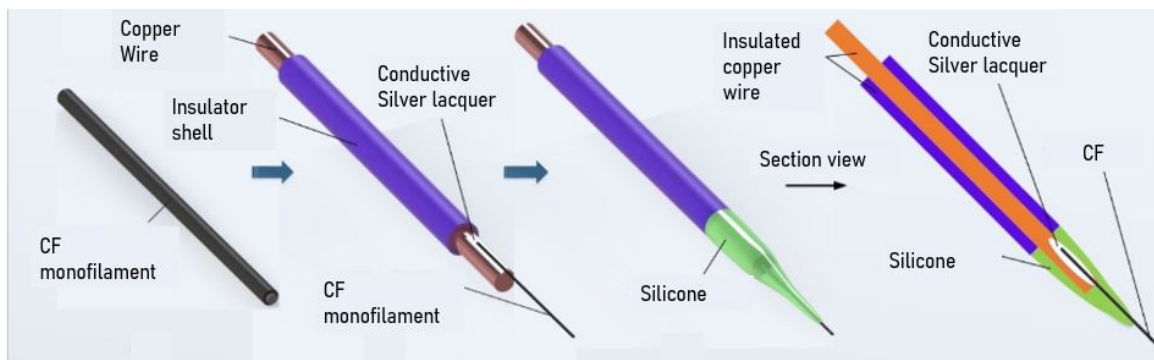

Figure 3.15: Diagram for the fabrication of a single electrode. Adapted from Lu et al.2017[45].

Figure 3.16: Left hand side:Electrodes for attaching CFs. Right hand side: Fibers attached to the electrode tip.

3.2 Equipment

3.2.1 Tubular furnace

The raw fibers were pyrolyzed using a tubular furnace OTF-1200X, which can be found in the School of Physical Sciences and Nanotechnology laboratory (figure 3.17).
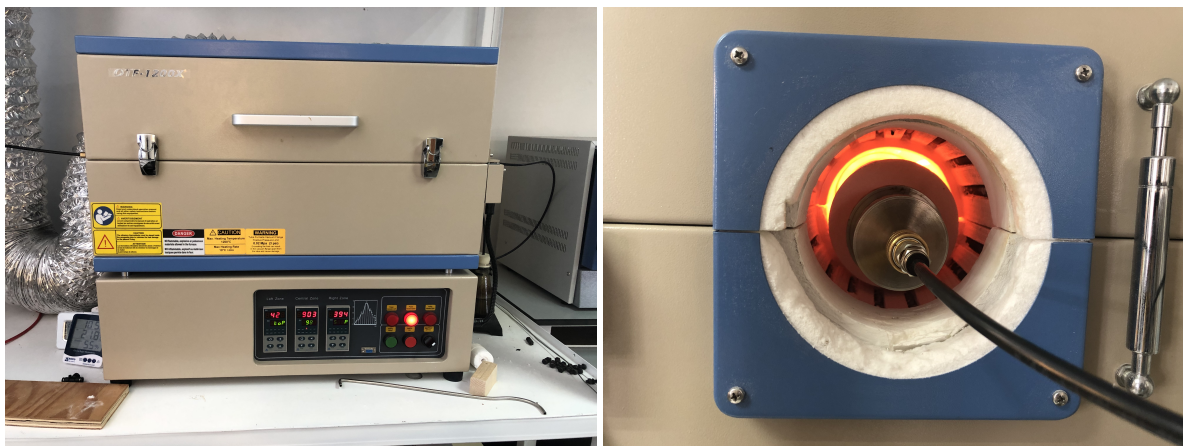

Figure 3.17: Tubular Furnace, OTF-1200X

3.2.2   SEM

A PHENOM ProX, with software pro suite detector fast SDD from AMPTEK located at the School of Earth Sciences, Energy and Environment, of Yachay Tech University(figure 3.18).

Figure 3.18: Scanning Electron Microscope, PHENOM ProX. Adapted from Yachay Tech web page. [90]

3.2.3 RAMAN

The Raman spectra were taken with a Raman spectrometer HORIBA LabRAM HR Evolution, belonging to Yachay Tech University, to the School of Physical Sciences and Nanotechnology (figure 3.19).
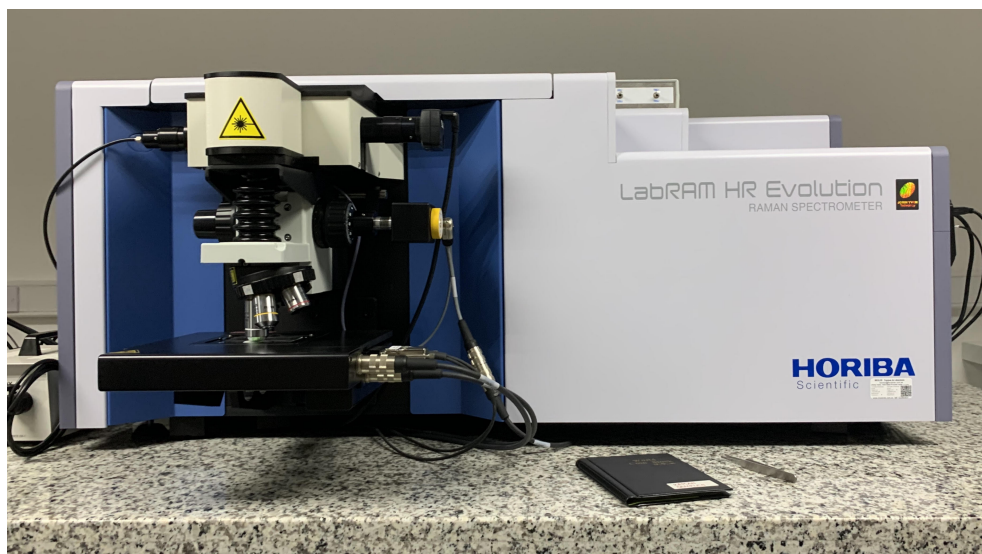

Figure 3.19: Raman spectrometer, HORIBA LabRAM HR Evolution.

3.2.4   XPS

The XPS spectres were taken by a PHI VersaProbe III from Physical Electronics Equipped with a 180 hemispherical electron energy analyzer. Monochromatized Al K_α source with energy 1486.6 eV, Survey operation energy bandpass: 255 kV High resolution for acquisition bandpass: 55 kV. Spot size diameter: 10 μm

The XPS belongs to Yachay Tech University, to the School of Physical Sciences and Nanotechnology (figure 3.20).
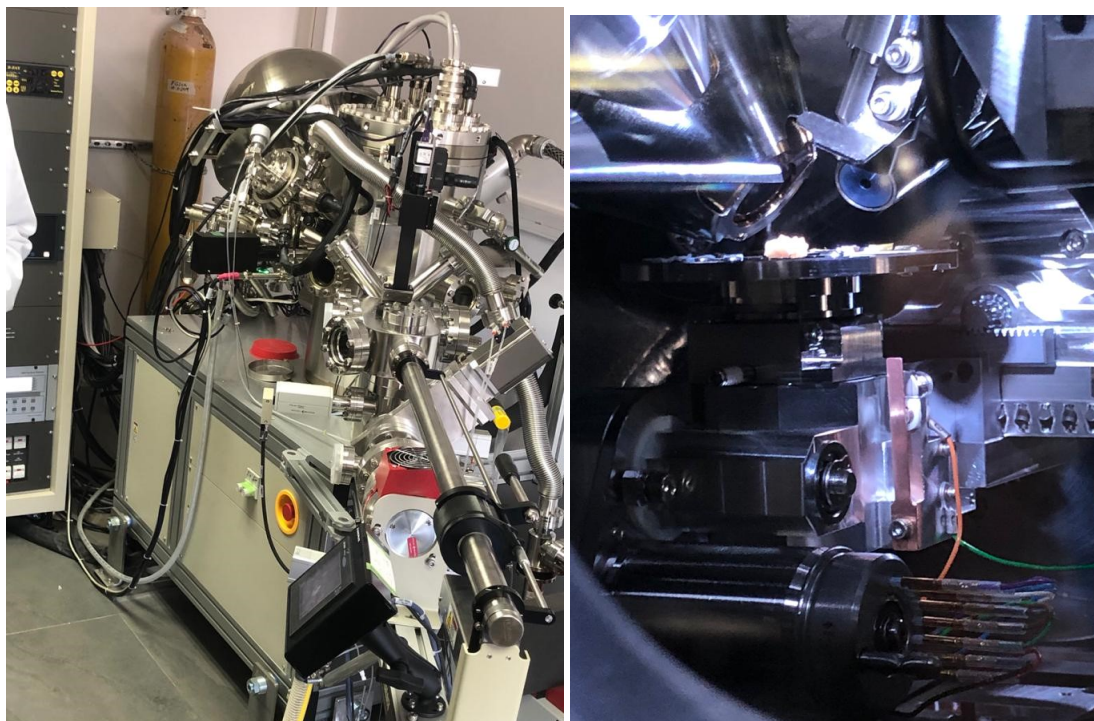

Figure 3.20: XPS, PHI VersaProbe III

3.2.5   FTIR

The infrared analysis of the samples was performed using an Agilent Technologies spectrometer Cary360 with a diamond attenuated total reflectance (ATR) accessory and resolution of 4 cm^{-1}, belonging to the School of Physical Sciences and Nanotechnology, of Yachay Tech University(figure 3.21).

Figure 3.21: FTIR instrument. Adapted from Agilent web page[91]

3.2.6   Potentiostat

CH Electrochemical Analyzer which belonging to Pontificia Universidad Catolica del Ecuador (PUCE) (figure 3.22).

Figure 3.22: Potentiostat, CH Electrochemical Analyzer.

3.3 Results & Discussion

3.3.1 Scanning Electron Microscopy (SEM)

The present micrographs belong to the batch two CFs and the size of CFs and naoparticles were measured with ImageJ software.

Carbon fibers

Figure 3.23 shows a micrograph from a top view where it can be appreciated two pyrolyzed fibers -without any further treatment- with diameters of about 30 and 21.4 μm respectively, a length bigger than 10 mm.
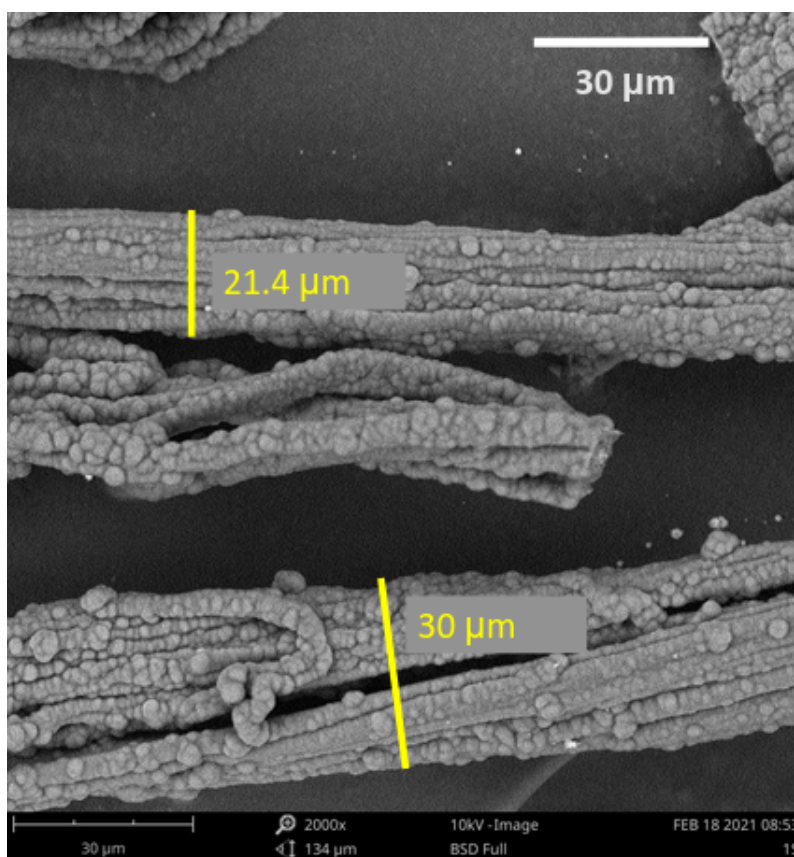

Figure 3.23: Carbon fibers

It can be denoted that the surface of the CFs is not homogeneous but show a topographic formed during the pyrolization process.

Xu et al., reported the use of PAN-based CFs with 6–8μm in diameter and 3 mm in length supplied by Jillin Carbon Group Co., Ltd[92]. Alternatively, Karacan et al., reported the size of a commercial fiber: Original New Star® meta-aramid multifilament yarn manufactured by Yantai Spandex Co. Ltd. (China), whose diameter was about 14.36μm and the diameters were uniform along the fiber axis direction. On the other hand, Li et al., reported the use of a highly porous, three-dimensional fibril-like network carbon fiber with average diameters of about 20 μm[93]. In contrast with this work, the diameter of BBCFs (between 20 and 30μm) were bigger, then the biomass-based CFs demonstrated competitiveness in terms of fiber size[79].

Besides, unlike the results obtained by Subramanian et al, where they obtained a micrometer-sized tube-like structure, the CFs presented in this work showed a better fiber structure[26].

Functionalized CFs

Figure 3.24 show micrographs of functionalized CFs where it can even clearly appreciated that CFs, in turn, are made up of fibers smaller in diameter. These small fibers can vary their size from 3.6 to 6.7 [μm]. Besides, the superficial structure of functionalized CFs shows not to be homogeneous and still seem to be just pyrolyzed CFs like Figure 3.23, even after being treated with concentrated H_2SO_4 and HNO_3 acids, the surface does not show a significant visible change.
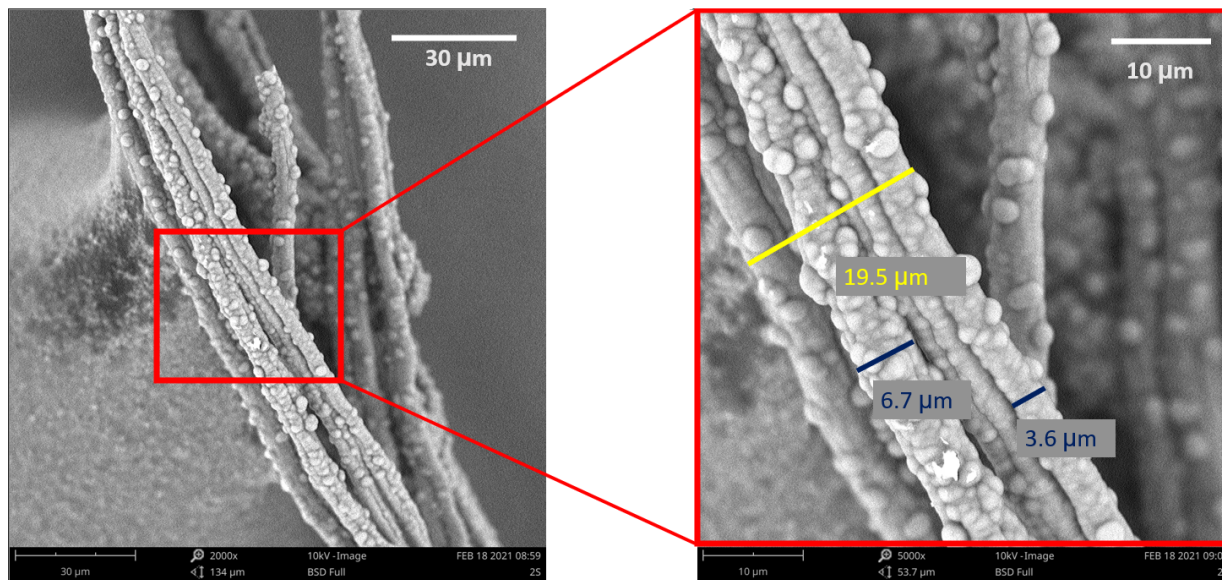

Figure 3.24: Functionalized carbon fibers

CFs decorated with Au NPs.

Figure 3.25 Show the micrographs of functionalized CFs decorated with Au NPs. It can be observed the Au NPs distribution, and also the formation of clusters. NPs average size is about 30nm (this taking into account some single NPs that are individually located in the fiber), and the NPs forming clusters of about 80 nm.
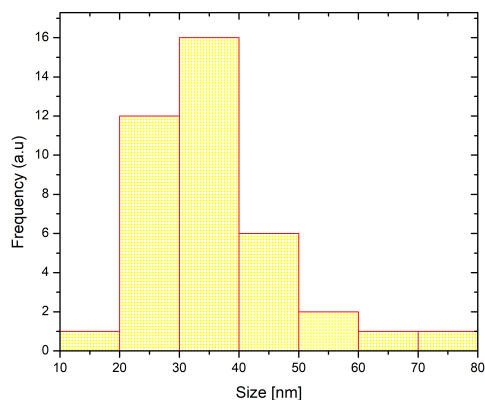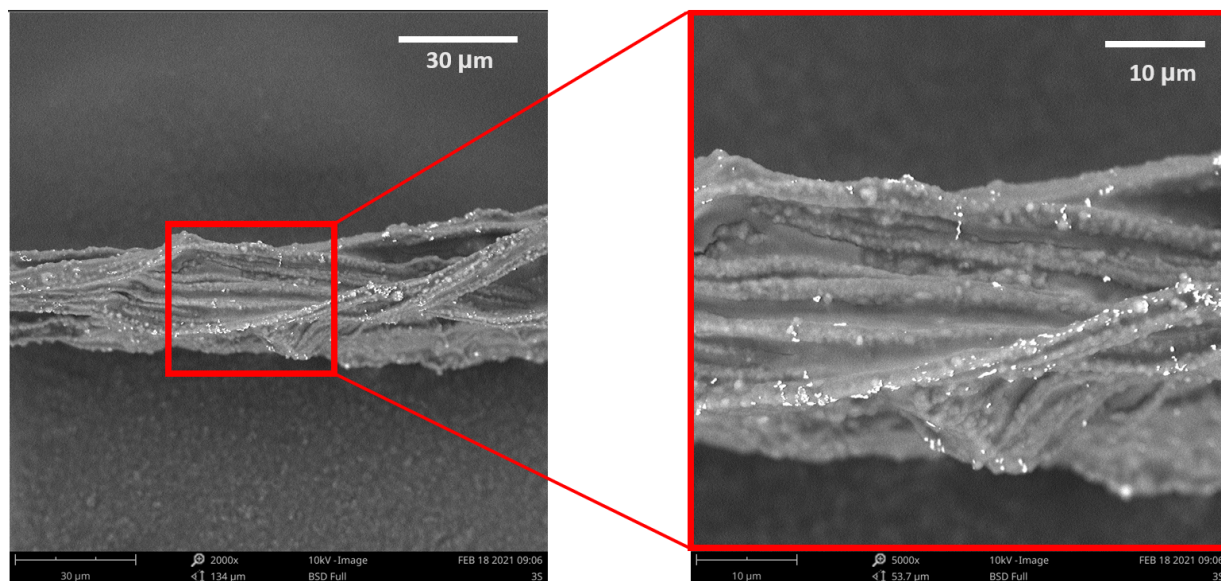

Figure 3.25: Carbon fibers decorated with Au NPs.

Li et al., decorated carbon fibers with Au NPs, whose size was about 12 nm, they immersed the CFs into the solution for overnight and then dried dried at 80 °C. The result, was similar to the presented in figure 3.25 where

white beads were uniformly distributed on the surface of CF indicating the strong adsorption of Au NPs [93].

CFs decorated with Ag NPs.

In Figure 3.26, unlike Figures 3.23 and 3.24, it is observed a long fiber composed of smaller fibers and even small clusters of NPs and NPs alone are distinguished, there is a dispersion not so good, but the presence of NPs is still distinguished. Nanoparticles (or clusters) size varies between 20 and 100 nm with an average of 50 nm, the presence of NPs is indisputable.

Figure 3.26: Carbon fibers decorated with Ag NPs.

CFs decorated with CeO$_2$ NPs.

In the micrograph 3.27 it is complex to visualize the deposition of nanoparticles since the size of each one of them is about 10 nm, and the SEM resolution does not present that resolution; therefore, it is complicated to observe and measure NPS.
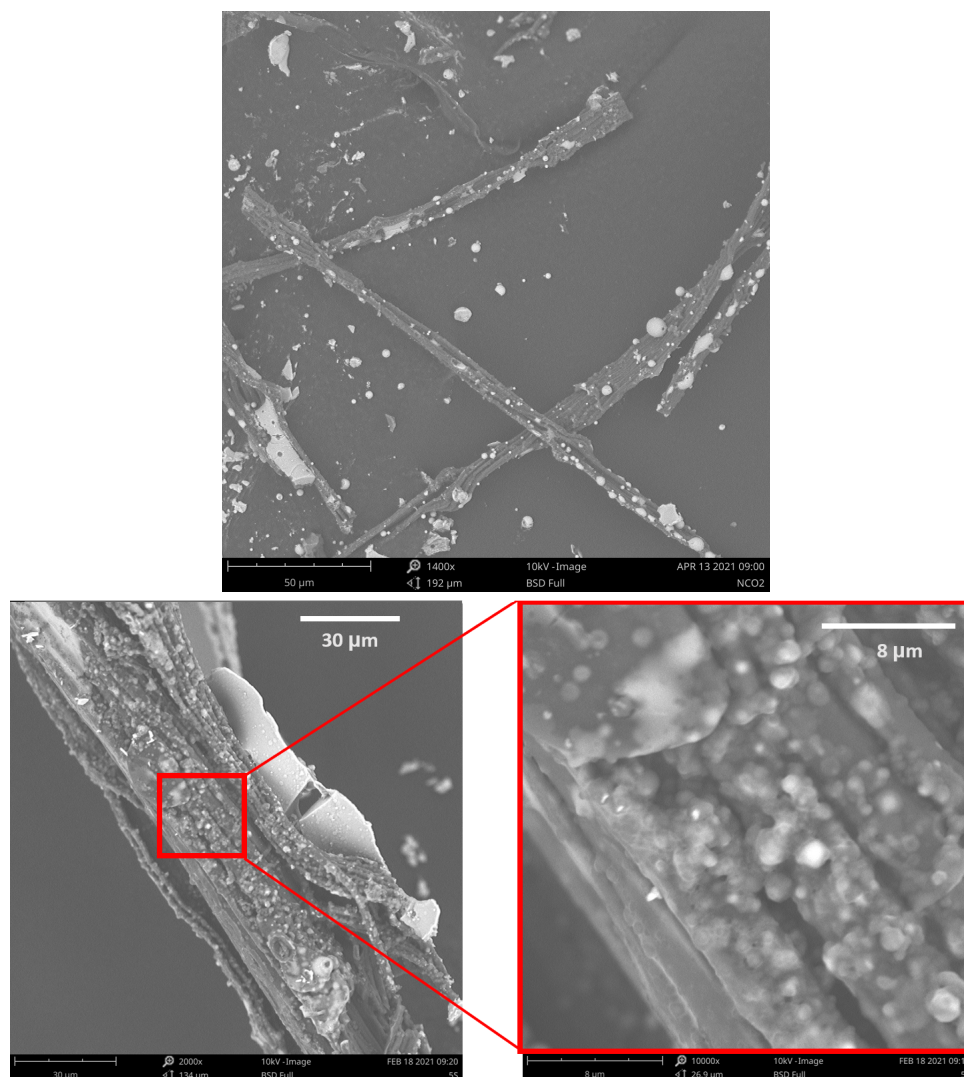
Figure 3.27: Carbon fibers decorated with CeO$_2$ NPs.

CFs decorated with AuFe$_3$O$_4$ NPs.

In Figure 3.28, it is observed a long fiber composed of smaller fibers and even small clusters of NPs and NPs alone are distinguished, there is a dispersion not so good, but the presence of NPs is still distinguished. Nanoparticles (or clusters) size varies between 20 and 100 nm with an average of 50 nm, the presence of NPs is indisputable.
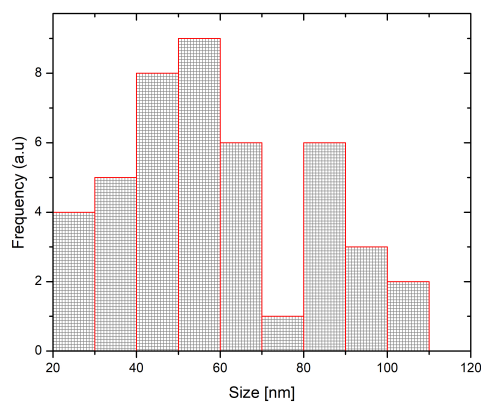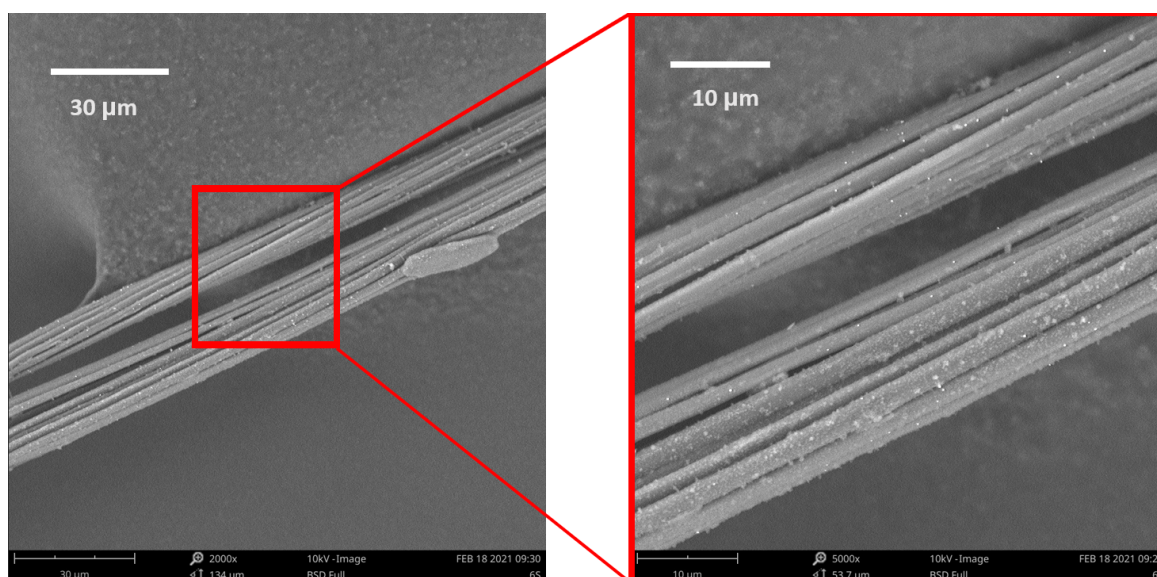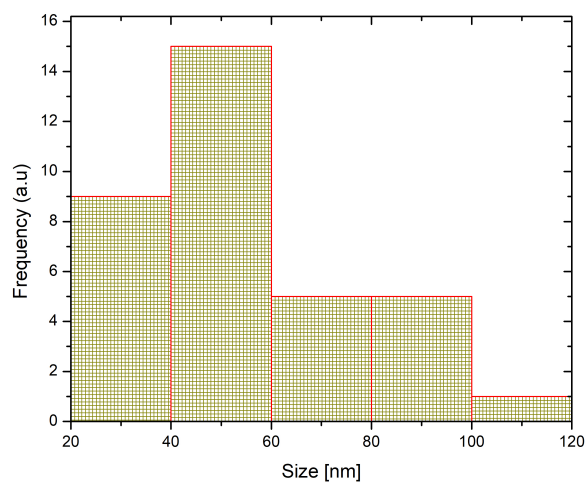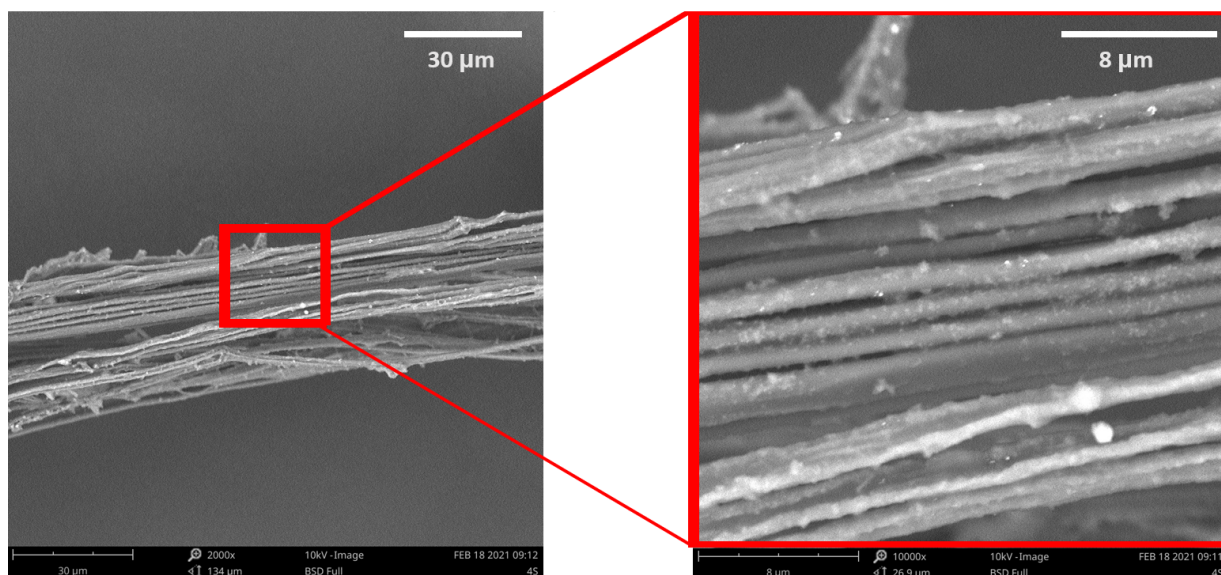

Figure 3.28: Carbon fibers decorated with AuFe$_3$O$_4$ NPs.

CFs decorated with CoFe$_2$O$_4$ NPs.

Figure 3.29 shown a smooth surface which is consistent with Liu et al., where reported a small size of NPs present on carbon fibers after an immersion process and subsequent pyrolization. It also agrees that Co NPs are relatively dispersed in very low concentration in this work[89].
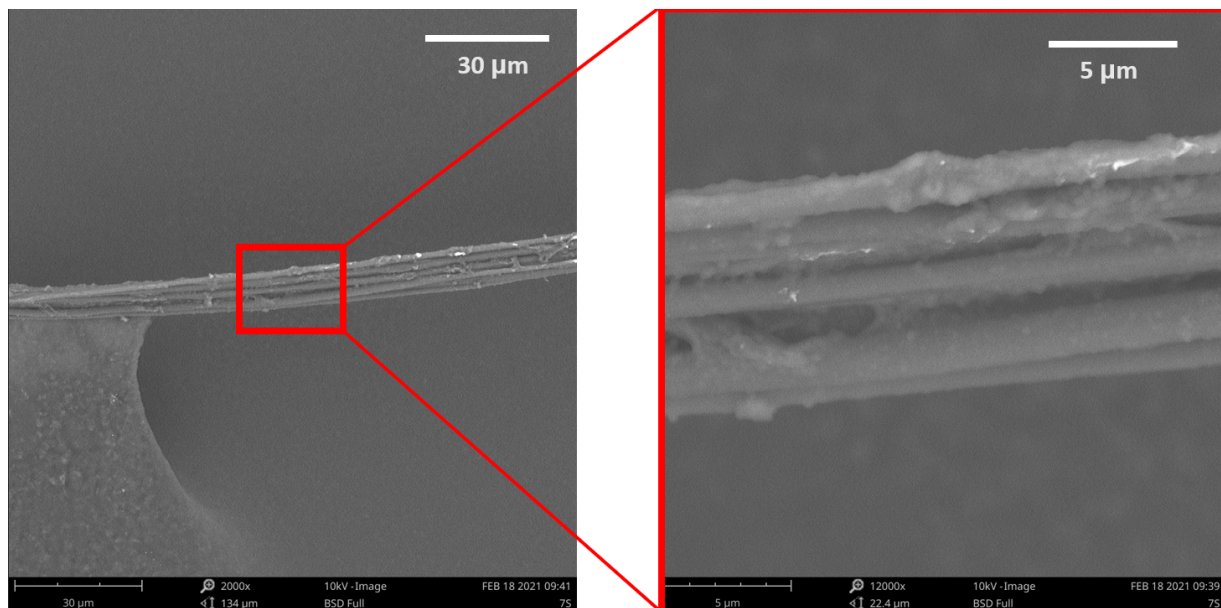
Figure 3.29: Carbon fibers decorated with CoFe$_2$O$_4$ NPs.

3.3.2   RAMAN

Raman spectroscopy was used to determine the degree of structural ordering in the CF samples.

Batch One

Carbon fibers decorated with Au and CeO$_2$ NPs, along with the pyrolyzed CF, had two typical Raman peaks ranging from 1000 to 1800 cm^{-1}. The peak located at approximately 1330 cm^{-1}, ascribed to a D band, which belonged to a sp^2 hybridized carbon, and the other peak located at approximately 1580 cm^{-1} was assigned to a G band[94]. The raman spectra can be appreciated in Figure3.30.

A narrowing of the breadth of the Raman bands (Fig. 3.30) is attributed to the structural arrangement or ordering of elemental carbon when the CFs are decorated with nanoparticles.
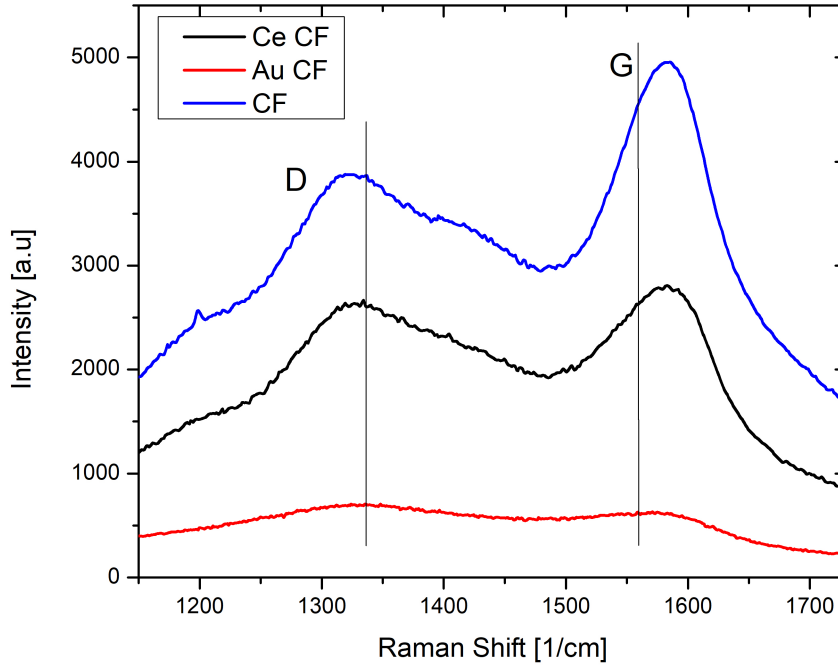
Figure 3.30: Raman spectrum of CF, and CFs decorated with Au and CeO_2 NPs.

Fiber	Peak Position		Peak Intensity		$R=I_D/I_G$
	D-Band	**G-Band**	**D-Band**	**G-Band**	
CF	1321.3	1584.8	3874.4	4956.1	0.78174371
CeO_2	1333.9	1583.1	2664.8	2806.6	0.94947623
Au	1335.7	1559.1	706.93	632.4	1.11785262

Table 3.5: Peak Position, Peak Intensity, and R(= I_D/I_G) Values of the First-order D and G band belonging to the pyrolyzed CF and CFs decorated with Au and CeO_2 NPs.

The I_D/I_G values of CFs decorated with Au NPs (see Table 3.5 was much higher than that of the CF decorated with CeO_2 NPs (0.95) and the Pyrolyzed CF (0.78) respectively, indicating an increase of disordered carbonous defects, see Table 3.5. The reason is that the decorating CF with nanoparticles gave the CFs more defects and disorders and thus led to the increase of its I_D/I_G value[75].

Batch Two

The raman spectra appreciated in Figure3.31 show the presence of the D and G bands of a, single CF, functionalized CF and functionalized CFs decorated with NPs. A narrowing of the breadth of the Raman bands (Fig. 3.31)is attributed to the structural arrangement of elemental carbon when the CFs are decorated with nanoparticles.

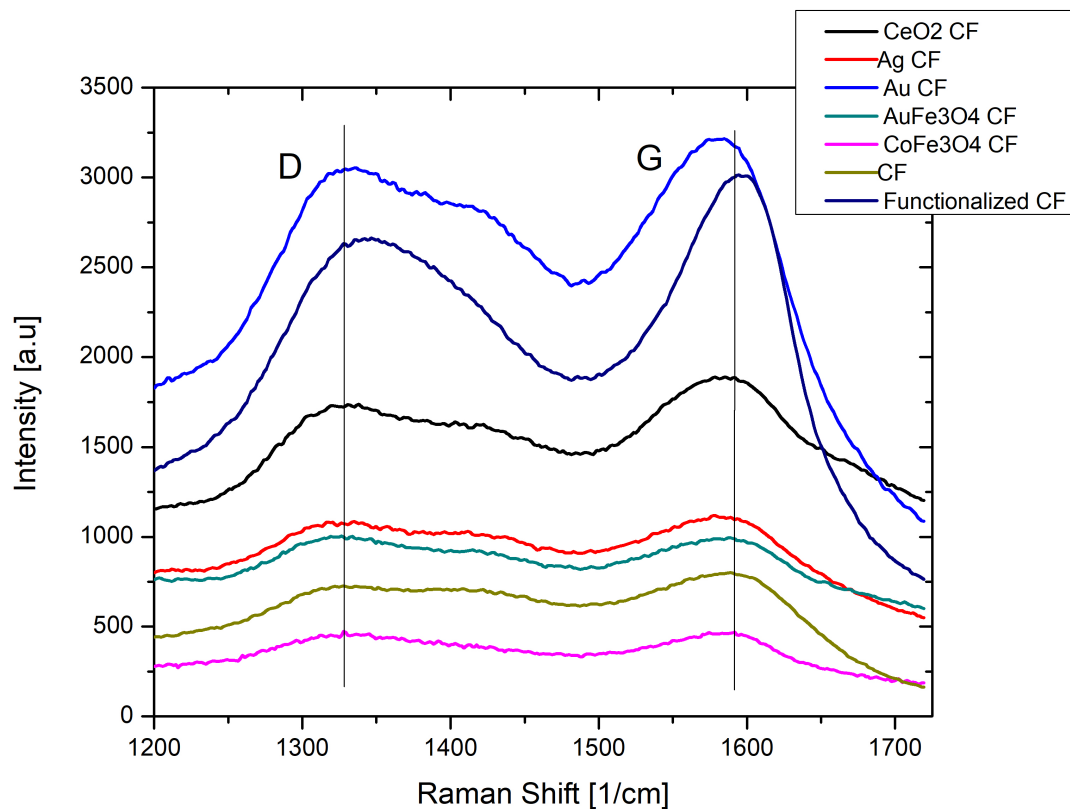Figure 3.31: Raman spectrum of CF, Functionalized CF and Functionalized CFs decorated with Au, Ag, CeO_2, $AuFe_3O_4$ and $CoFe_2O_4$ NPs.

Fiber	Peak Position		Peak Intensity		R=I_D/I_G
	D-Band	G-Band	D-Band	G-Band	
CF	1327.4	1588.3	727.05	802.02	0.90652353
Functionalized	1347.3	1594.3	2664.4	3018.2	0.88277781
Au	1335.1	1583.6	3056.2	3216.9	0.95004507
CeO_2	1337.5	1585.3	1741.4	1892.6	0.9201099
Ag	1317.9	1577.7	1079.8	1118.6	0.96531379
$AuFe_3O_4$	1333.2	1588.8	1004.1	994.48	1.0096734
$CoFe_2O_4$	1328.3	1590.5	473.26	465.9	1.01579738

Table 3.6: Peak Position, Peak Intensity, and R(= I_D/I_G) Values of the First-order D and G band.

The I_D/I_G values (see Table 3.6) of CFs decorated with $CoFe_2O_4$ (1.01) and $AuFe_3O_4$ NPs (1.01) were much higher than that of the CFs decorated with Ag (0.96) and Au (0.95) NPs. The CeO_2 (0.92) and the pyrolyzed CF (0.90) is closer to the Pyrolyzed CF (0.78), and the most interesting ratio is the one of the Functionalized CF (0.88). Indicating that the $AuFe_3O_4$ and $CoFe_2O_4$ leads to an increase of disordered carbonous defects, whereas the functionalization process shows less disordered carbonous defects in comparison with any other fiber of batch two. This because, decorating the CFs with nanoparticles gave the CFs more defects and disorders and thus led to the increase of its I_D/I_G value[75].

When Raman spectra from batch one and batch two were compared, it was found that the CF from batch one had an R-value of 0.78, whereas the CF from batch two had an R-value of 0.90. Being that batch one was pyrolyzed at 600 °C, and on the other hand, batch two was pyrolyzed at 1000 °C, this temperature change is reflected in the shift of the G-band from 1584 to 1588 cm^{-1} between 600 and 1000 °C, respectively. Which can be attributed to the growth of sp^2-bonded crystalline carbons at higher temperatures[79]. For both batch one and two (Figs. 3.30 and 3.31), the breadth of the same band became narrower, indicating a decrease of order in the carbon fiber structure when the CFs are decorated.

When compared PAN and biomass-based CFs obtained in this work, Zhang et al reported in their work of "The surface analytical characterization of carbon fibers functionalized by H_2SO_4/HNO_3 treatment" that functionalization treatment has caused large increases between the band intensities[58], which is consistent with the results above presented.

3.3.3 XPS

The XPS technique's contribution in this work is the precise identification of the elements present on the surface of the single CF and the decorated CF samples.

Batch One

As shown in the survey spectras (Figure 3.32), all (a,b,c,d,e) CF samples exhibited two prominent peaks with binding energies around 530 and 283 eV, which belongs to the presence of C1s, respectively, suggesting an effective carbonization[31]. From Fig. 3.32, the significant peaks in the spectra were due to the C1s and O1s, and a smaller N1s peak is also discernible. In contrast, the peaks around 400eV, corresponding to N1s, was observed clearly for the sample a and b.

The CF sample (Fig. 3.32a) showed prominent peaks belonging to Na, O and C, whereas the CF decorated with CeO_2 (Fig. 3.32b) showed two more peaks which correspond to Ce. On the other hand, the CF decorated with Au NPs (Fig. 3.32c) besides of showing the Au corresponding peaks, also it was discernible the presence of a N corresponding peak, due to the NPs synthesis method. The CF decorated with $AuFe_3O_4$ (Fig. 3.32d)showed prominents peaks belonging to O, Au, O and C. The $CoFe_2O_4$ (Fig. 3.32e) showed peaks corresponding to Na, Co, $CoFe_2O_4$ (according to NIST XPS Database), O and C.

This is most readily seen in Table 3.7, which contains the atomic percentages (in %) of the various elements, as determined from the spectral areas and relative sensitivity factors.

The percentage of Carbon present was the highest for both the Pyrolyzed CF and the CF decorated with CeO_2 NPS, with 70.1 and 70.5% respectively. The percentage of Oxygen present in the CF decorated with $CoFe_2O_4$ was the highest with 37.4%, followed by the CF decorated with $CoFe_2O_4$ NPs with 30.1%. A smaller percentage of N1s presence is discernible just for Au and the CeO_2 decorated CFs, with 2.6 and 1.1%, respectively. Also, a small presence of Na is also discernible as part of the CF with 1, 1.6, and 1.8% for the pyrolyzed CF and the Au, $CoFe_2O_4$ decorated NPs.

It is apparent that C was the most dominant constituent in all samples, and O was the second. When decorating with NPS, oxygen content increased from 27.5% for the CF to 37.4% for the $CoFe_2O_4$. Simultaneously, the carbon content decreased from 70.1% for the pyrolized CF to 57.7% for the the $CoFe_2O_4$ decorated CF. It is important to clarify that the content of C was similar for the pyrolyzed CF and the CF decorated with CeO_2 NPs.
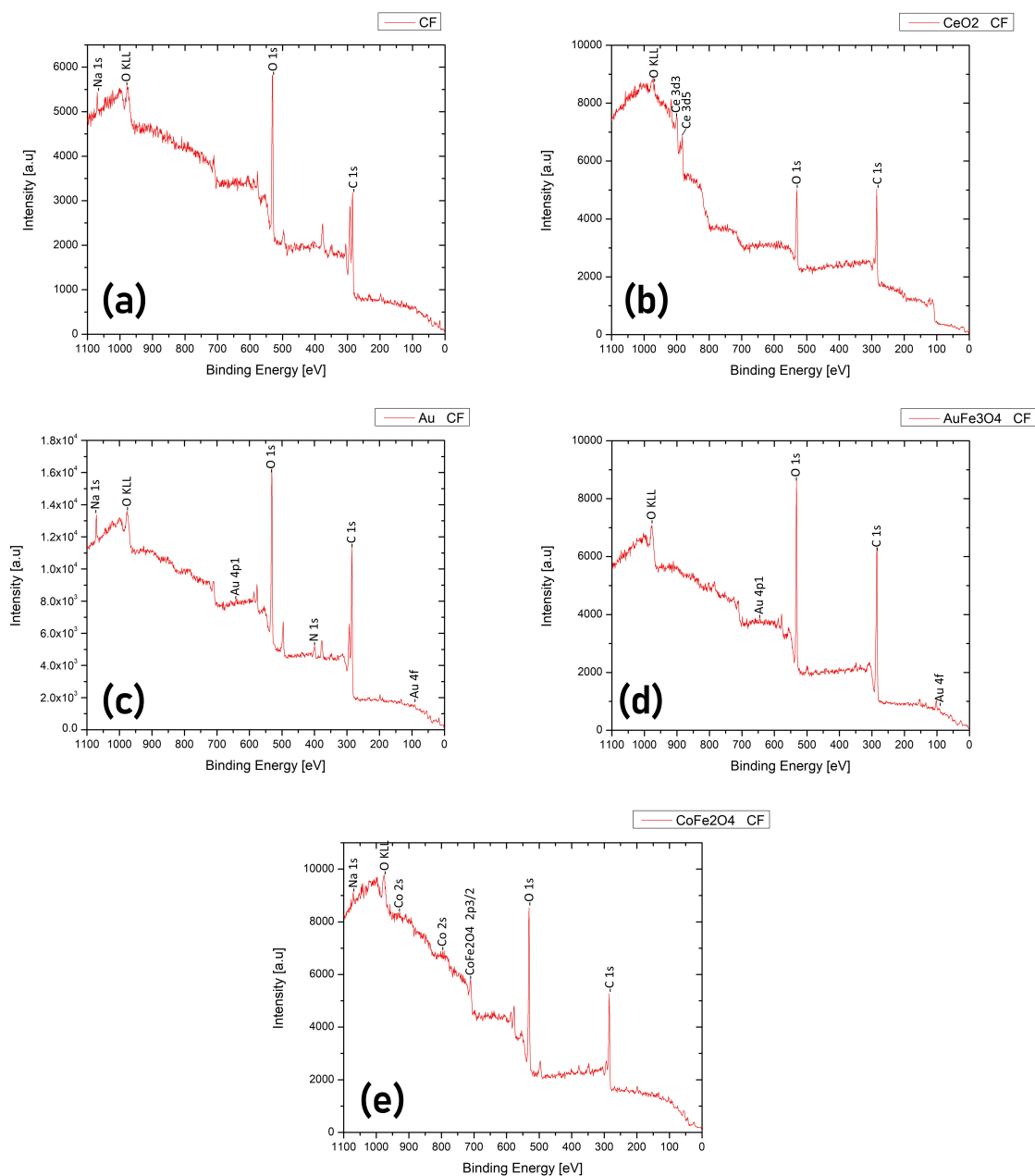
Figure 3.32: XPS analysis of (a) single Carbon fiber, (b) CF decorated with CeO_2 NPs, (c) CF with Au NPs,(d) CF decorated with $AuFe_3O_4$ NPs, (e) CF decorated with $CoFe_2O_4$ NPs.

Fiber	C (%)	O (%)	Na (%)	N (%)	Au (%)	Ce (%)	Co (%)
CF	70.1	27.5	1				
Au CF	67.7	26.7	1.6	2.6	0.1		1.4
CeO$_2$ CF	70.5	25.3		1.1		1	
AuFe$_3$O$_4$	67.8	30.1					
CoFe$_2$O$_4$	57.7	37.4	1.8				

Table 3.7: Elemental composition of Pyrolyzed and CFs decorated with NPs.

Batch Two

It can be appreciated in Figures 3.33 and 3.34 the survey spectras of all (a,b,c,d,e,f,g,h) fiber samples exhibited two prominent peaks with binding energies around 530 and 283eV, which belongs to the presence of O1s and C1s, respectively. From Fig. 3.33, it can be appreciated a notorious difference between the raw fiber and the pyrolyzed fiber. The CF showed a bigger intensity in the zone 1100-700eV.

The raw fiber (Fig. 3.33a) showed peaks belonging to O, C, N and even Si. The CF sample (Fig. 3.33b) showed prominent peaks belonging to Na, O and C, whereas the functionalized CF (Fig. 3.33c) showed a more visible peak belonging to Na besides a N and S peak, and of course the common O and C peaks. On the other hand, the CF decorated with CeO$_2$ NPs (Fig. 3.33d) besides of showing the O and C peaks, it also was discernible the presence of a N corresponding peak, and the Ce peaks.

The functionalized CF decorated with Au NPs (Fig. 3.34e) showed the common O and C peaks, and also Na, N and Au peaks were present. The functionalized CF decorated with Ag (Fig. 3.34f) showed the characteristic O and C peaks, and also a discernible Ag and Na peaks. In contrast, the functionalized CF decorated with AuFe$_3$O$_4$ (Fig. 3.34g) showed Au, Fe, S and Na peaks, besides of the well known C and O peaks. Regardless the CoFe$_2$O$_4$ (Fig. 3.34h), besides of the known O and C peaks, it also was visible the presence of Na, Co, CoFe$_2$O$_4$, N and S corresponding peaks.

The elemental composition (in %) on the raw, CF, functionalized Cf and functionalized decorated CF samples were summarized in Table 3.8. The percentage of Carbon present was the highest for both the functionalized CF decorated with Au NPs and the functionalized CF decorated with CeO$_2$ NPS, with 72.1 and 70.5% respectively. The percentage of Oxygen present in the CF decorated with Ag NPs was the highest with 41.1%, followed by the single CF with 39.7%. A smaller percentage of Au is discernible just for the functionalized CFs decorated with Au and AuFe$_3$O$_4$ NPs, with 0.1 and less than 0.1%, respectively.

In a study conducted by Zhang, et al. XPS analysis of a PAN fiber resulted in an atomic percentage of 98.8% C and 1.1% O. Since poly(acrylonitrile)-PAN- retains residual N and polysaccharides retain residual O, the absence of residual oxygen in the PAN sample means that pitch is the source. When the elemental composition of te surface of biomass-based CFs are compared with PAN carbon fibers, the difference is huge, the PAN is composed by C and O whereas the biomass-based Cfs were composed of C an O, but also presented other species[58].

At the time of functionalize the PAN fibers, the percentage of C was decreased, and on the other hand the

percentage of O increased. Depending on the volume ratio of H_2SO_4/HNO_3 employed, they found that: When a volume ratio of 3:1 was used, the amount of C decreased to 81.3% and the amount of oxygen increased to 16.4%, and an atomic percentage of 1% S and 1.3% N, were also present on the fiber surface.

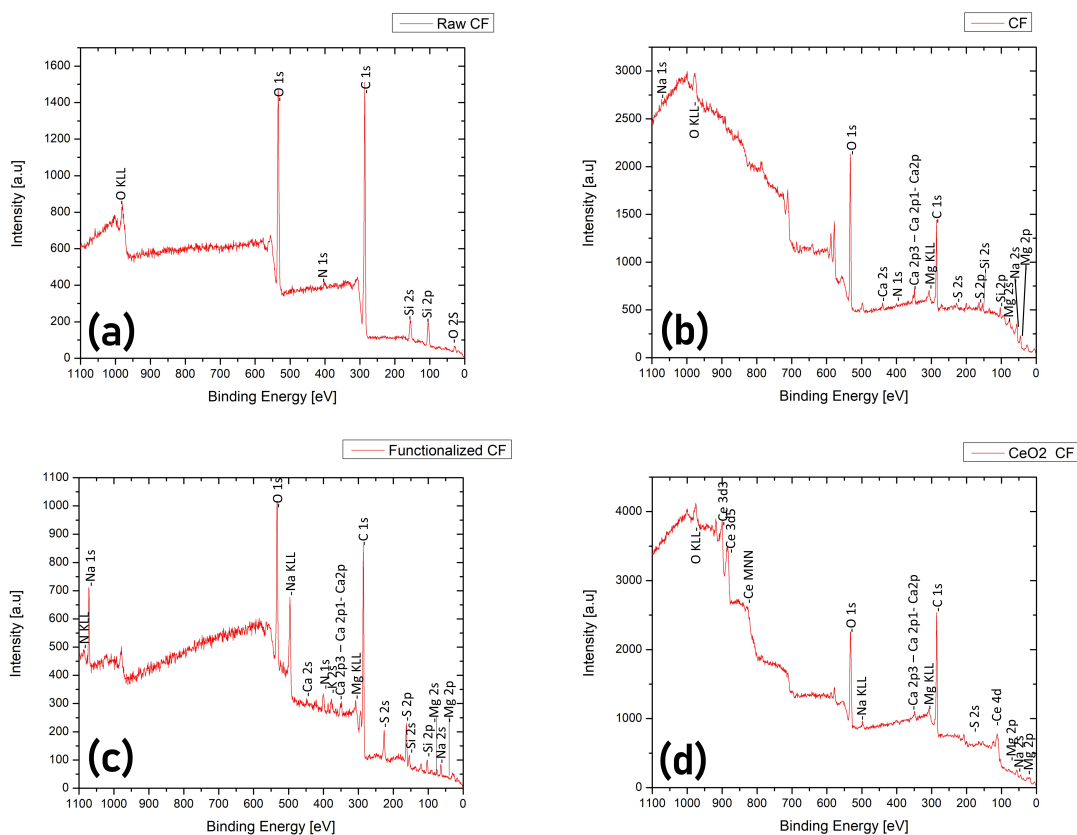Figure 3.33: XPS analysis of (a) Raw fiber, (b) single Carbon fiber, (c) Functionalized CF, and (d) Functionalized CF decorated with CeO_2 NPs.
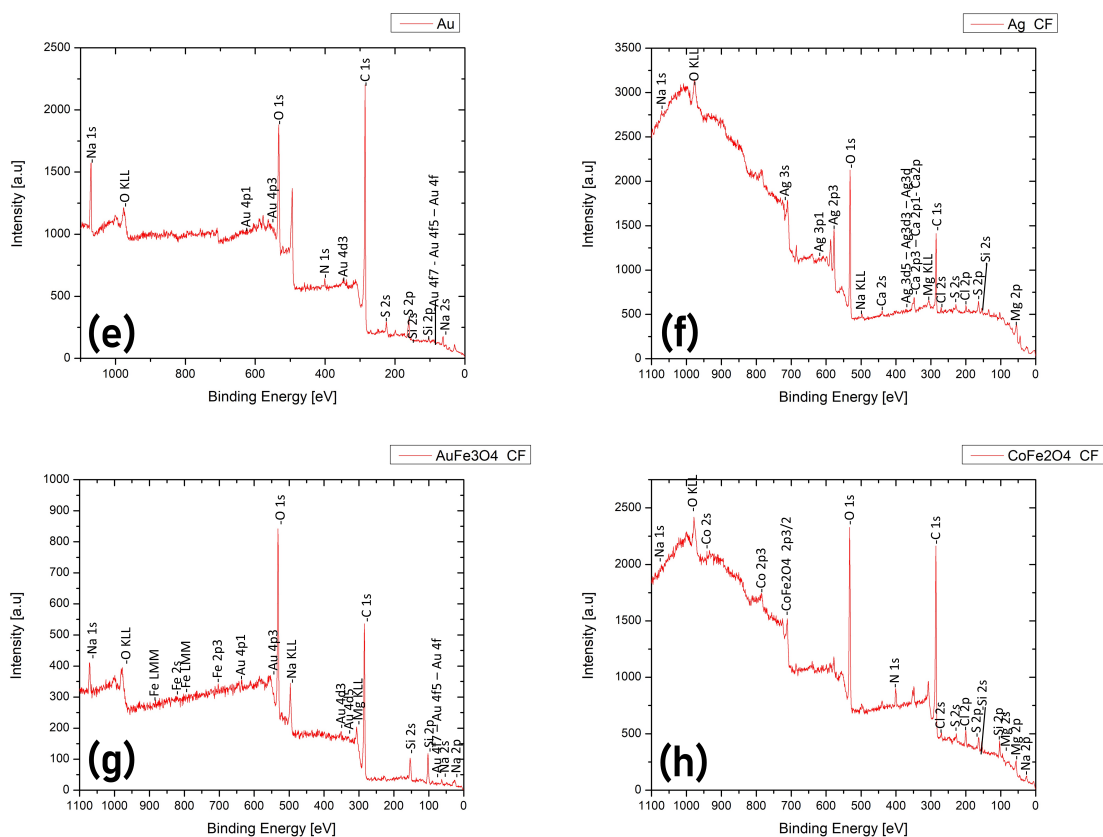
Figure 3.34: XPS analysis of (e) Functionalized CF decorated with Au NPs, (f) Functionalized CF decorated with Ag NPs, (g) Functionalized Carbon Fiber decorated with $AuFe_3O_4$ NPs, and (h) Functionalized carbon fiber decorated with $CoFe_2O_4$ NPs.

Fiber	C (%)	O (%)	Na (%)	N (%)	S (%)	Au (%)	Ag (%)	Ce (%)	Co (%)
Raw	65.2	26.6		1.6					
CF	48	39.7	0.9	1.3	0.4				
Functionalized	61.9	21.7	3.8	4.8	2.9				
Au CF	72.1	17.4	5.6	1.7	2.2	0.1			
Ag CF	42.9	41.1	< 0.1		2.8		< 0.1		
CeO$_2$	70.5	25.3		1.1				1	
AuFe$_3$O$_4$	56.5	31.3	4.1			< 0.1			
CoFe$_2$O$_4$	63.9	24.7	0.8	3.8	0.9				1.2

Table 3.8: Elemental composition of raw, pyrolyzed and functionalized CFs decorated with NPs.

High Resolution Analysis

Figures 3.35 and 3.36 show the fitting of C1s region. Four main peaks were found with binding energies of around 289, 286, 285 and 284, which correspond to functional groups of O-C=O, C-O, C-C and C=C[31,95,96].

The raw fiber (3.35a) presented three peaks, at 289, 286.4 and 284.6, which correspond to O-C=O, C-C and C=C respectively.

The single CF (3.35b) presented two peaks, at 286.8 and 285.6, corresponding to C-O and C-C.

In contrast the functionalized CF (3.35c) presented three peaks of around 289.9, 285.7 and 284.4, belonging to O-C=O, C-C and C=C respectively.

The functionalized CF decorated with Ag NPs (3.35d) presented two peaks, the first peak at 286.6 and the second one at 285.2, corresponding to C-O and C-C respectively.

The functionalized CF decorated with CeO$_2$ NPs (3.36e) presented two peaks, at 286.1 and 284.8, belonging to C-C and C=C repectively.

The functionalized CF decorated with Au NPs (3.36f) presented two peaks at 287.5 and 285.5 corresponding to C-O and C-C respectively.

The functionalized CF decorated with AuFe$_3$O$_4$ NPs (3.36g) presented three peaks at 286.4 and 284.9 and 283.8, corresponding to C-O, C-C and C=C respectively.

Finally, the functionalized CF decorated with CoFe$_2$O$_4$ NPs (3.36h) presented three peaks at 289.3 and 287.5 and 284.9, corresponding to C-O, C-C and C=C respectively.

The presence of edge and defect sites on the graphitic surface provides ideal anchoring sites for the functionalities, forming the C-H bond and oxygen-containing bonds. Furthermore, since the C-O and C=O peaks cannot be resolved in the results, they are combined into a single peak[95].

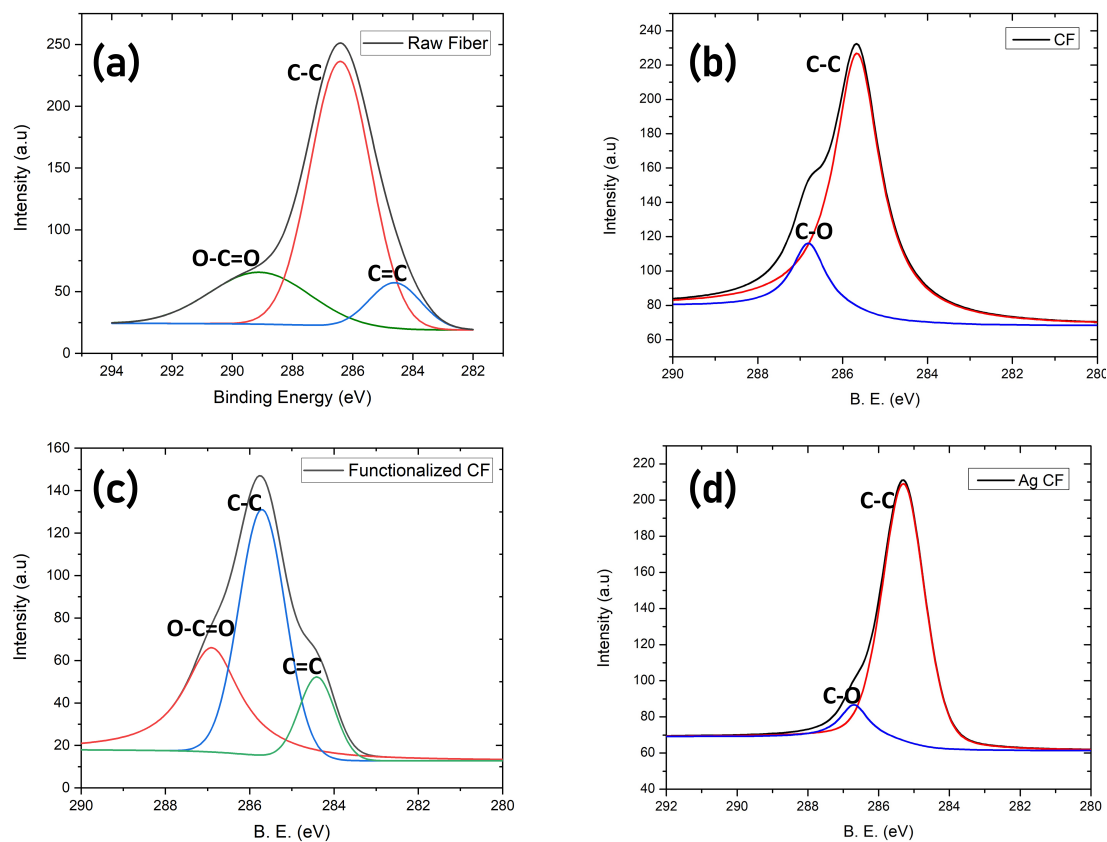Figure 3.35: High resolution XPS of C1s (a) Raw fiber, (b) single Carbon fiber, (c) Functionalized CF, and (d) Functionalized CF decorated with CeO_2 NPs.
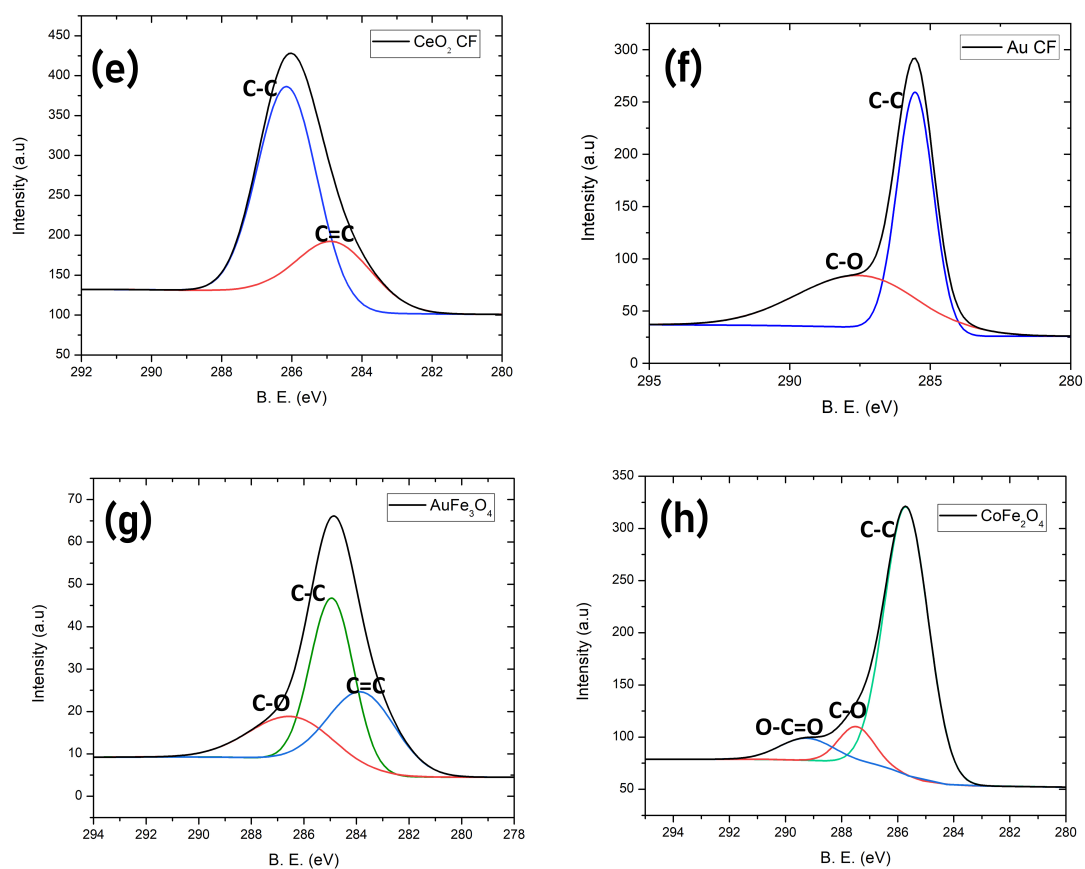
Figure 3.36: High resolution XPS of C1s (e) Functionalized CF decorated with Au NPs, (f) Functionalized CF decorated with Ag NPs, (g) Functionalized Carbon Fiber decorated with $AuFe_3O_4$ NPs, and (h) Functionalized carbon fiber decorated with $CoFe_2O_4$ NPs.

3.3.4 FTIR

The chemical structure and functional groups of CFs can be determined by Fourier transform infrared (FTIR) spectroscopy. The FTIR spectra of the Pyrolyzed and functionalized CFs are shown in Fig. 3.37 In the FTIR spectra (Figure 3.37), it was observed an absorption peak at 3500-3200 cm^{-1} and was assigned to the -OH stretching vibration of hydroxyl, while those of 2700-2500 cm^{-1} were assigned to the C–H bond stretching vibrations. The C=C bond stretching vibration resulted in an absorption peak at 1700-1500 cm^{-1}, and the absorption peak at 1500-1000 cm^{-1} was attributed to the stretching vibration of the C-O bond[31,86,97]. C=C bond stretching vibration and C-O bond were present in all CFs as shown in Table 3.9. Besides, the FTIR spectrum of the functionalized CF decorated with Au NPs, has a weak absorption peak at 617 cm^{-1}.

Overall, the resultant CFs may contain hydroxyls, –CH$_2$– or –CH$_3$, C=C, C–O and other chemical groups[31].

The presence of a new O-H group is distinguished after functionalizing in all the CFs samples compared to the unfunctionalized CF (Fig.3.37d) and also may be attributed to the presence of water which was the solvent used for decorated the CFs with NPs. The CF functionalized and decorated with Au NPs (Fig. 3.37a) is the one that shows the greatest intensity in its peaks, and where it is easier to make a comparison with respect to pyrolyzed CF (Fig.3.37d). So much so that the presence of functional groups (see Table 3.9) is indisputable in this fiber. So,the abundant presence of O functional groups in the prepared materials can facilitate the electrode's wettability, leading to an effective mass transfer.[30]

The single CF (Fig. 3.37d) showed some peaks, but with low intensity compared to other fibers, however, such spikes were found at 2700, 1562 and 1000 cm^{-1}, where each peak has a corresponding functional group (see Table 3.9), which are the C-H, C=O and C-O respectively.

On the other hand, functionalized CF (Fig. 3.37e) showed the presence of 4 peaks located at 3270, 1558, 1384 and 1030 cm^{-1}. According to Mohamed, et al[86]. The peak at 3270 belongs to O-H functional groups, the peat at 1558 to N-H groups, the peak at 1384 to S=O or C-H groups and 1030 to C-O.

In contrast, the functionalized CF decorated with CeO$_2$, 2917 cm^{-1} to C-H or O-H, 2850 cm^{-1} to C-H or O-H, 1513 to C=C or N=O, 1410 to C-H or N=O and less than 500 cm^{-1} to C-X[86]. Due to the commercial origin of CeO$_2$ NPs it is not known what media they are in, but they are in an organic solvent and about 500 cm^{-1} it is present the metal-oxygen bond.

The functionalized CF decorated with Au NPs, peak at 3357 to O-H, peak at 2880 to C-H, peak at 1640 to C=C, 1580 to C=C or N-H, 1474 to C=C, 1043 to C-O and 617 to C-X[86].

The functionalized CF decorated with AuFe$_3$O$_4$ NPs, this fiber share the same peaks, just like the functionalized CF, where the peak at 3270 belongs to O-H functional groups, the peat at 1558 to N-H groups, the peak at 1384 to S=O or C-H groups and 1030 to C-O.

The functionalized CF decorated with CoFe$_2$O$_4$ NPs, showed peaks at 3260 belonging to O-H, 1573 belonging to C=C or N-H and 1030 belonging to C-O.

According to Perez de Berti et al., peaks at 2851–2853 and 2922–2925 cm^{-1} are attributed to the symmetric and asymmetric CH$_2$ stretching modes, respectively, and peaks at 3003–3006 cm^{-1} are attributed to the C–H bond adjacent to the C=C bond in both pure oleic acid and oleylamine used in the synthesis of CoFe$_2$O$_4$ NPs[98]. In addition Do et al., reported that the stretch modes of oleic acid -CH2$_2$- and -CH$_3$- are observed in the bands at 2862 and

2923. The band at 1438, 1518 was attributed to the asymmetric and symmetric stretching vibrations of the -COO-functional group, suggesting that a layer of oleic acid is coating the surface of NPs[99]. Also, oleylamine displays typical modes of amine groups: the peak at 1576 cm^{-1} is due to the NH_2 scissoring mode and the peak at about 3300 cm^{-1} is assigned to the N–H stretching mode[98].

According to Khoshnevisan et al., the two different CH bands vibration of CTAB (used in the synthesis of Au and $AuFe_3O_4$) can be found at 2848 and 2918 cm^{-1} [100].
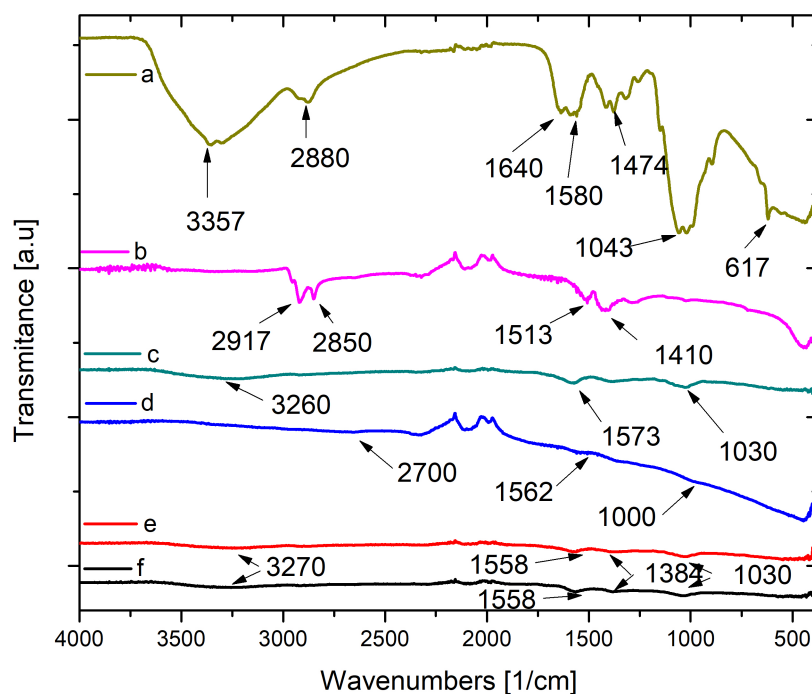
Figure 3.37: FTIR spectra of (a) Functionalized CF decorated with Au NPs, (b) Functionalized CF decorated with CeO_2 NPs, (c) Functionalized CF decorated with $CoFe_2O_4$, (d) Pyrolyzed CF, (e) Functionalized CF, and (f) Functionalized CF decorated with $AuFe_3O_4$ NPs.

Fiber	Peak Position	Bond
	2700-2500	C-H
CF	1700-1500	C=O, C=N, C=C
	1500-1000	C-O
	3500-3200	O-H
Functionalized	1700-1500	C=O, C=N, C=C
	1500-1000	C-O
	3500-3200	O-H
	3000-2800	C-H
Au	1700-1500	C=O, C=N, C=C
	1500-1000	C-O
	1000-500	C-H
	617	Au presence
	3000-2800	C-H
CeO$_2$	1700-1500	C=O, C=N, C=C
	1500-1000	C-O
	440	Ce presence
	3500-3200	O-H
AuFe$_3$O$_4$	1700-1500	C=O, C=N, C=C
	1500-1000	C-O
	3500-3200	O-H
CoFe$_2$O$_4$	1700-1500	C=O, C=N, C=C
	1500-1000	C-O

Table 3.9: FTIR peaks and related stretching vibrations.

3.3.5   Cyclic Voltammetry

The reference electrode employed for the CV was a silver/silver chloride (Ag / AgCl) due to its simplicity, inexpensive design, and non-toxic components. The standard potential of the Ag / AgCl electrode is E° Ag/AgCl = 0.222 V [101]. The counter-electrode was a graphite piece, and of course, the working electrode was the CF. The cell design where the electrodes were introduced is shown in Fig. 3.38

Figure 3.38: Cell design for CV.

The electrolyte, $K_4Fe(CN)_6$, were vacuumed to avoid side reactions between the carbon-based electrodes and O_2 dissolved in the solution. Figure 3.39 shows the CV curves of the as-prepared CF electrodes from four different fibers of the same batch in 5.0 mmol $K_4Fe(CN)_6$, performed at a scan rate of 0.10 V·s^{-1}

.
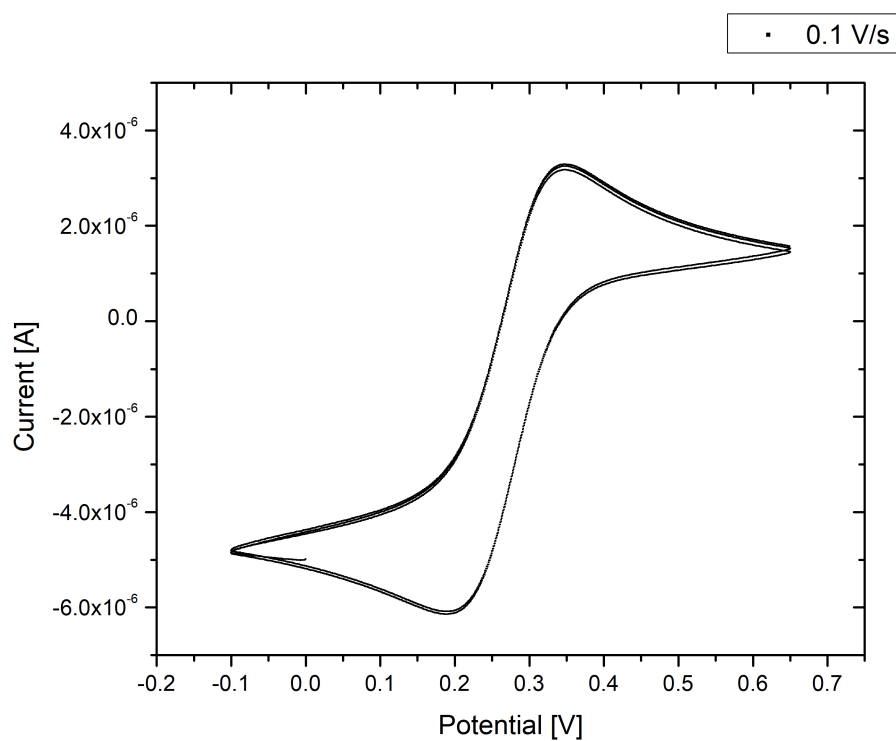
Figure 3.39: CV of a single CF in a 5.0 mmol $K_4Fe(CN)_6$ at a scan rate of 0.10 V·s≃1

Figure 3.39 shows the CV curve of a carbon fiber in 5.0 mM $K_4Fe(CN)_6$, performed at a scan rate of 0.10 V·s^{-1} As shown, the CV of the biomass-based CF, just like the PAN-based CF exhibits a highly symmetrical shape for both the forward and reverse potential scans, meaning that highly reversible redox reactions are taking place at the carbon fiber[88].
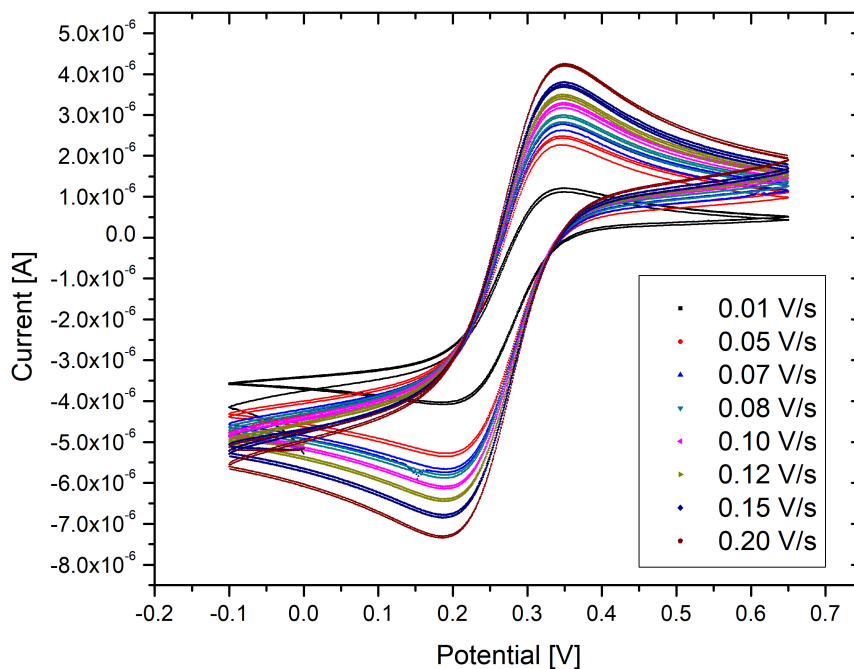
Figure 3.40: Cyclic voltammogram of a single CF at different scan rates: (a) in a 5.0 mmol $K_4Fe(CN)_6$ at a scan rate of 0.01 $V·s^{-1}$, 0.05 $V·s^{-1}$, 0.07 $V·s^{-1}$, 0.08 $V·s^{-1}$, 0.10 $V·s^{-1}$, 0.12 $V·s^{-1}$, 0.15 $V·s^{-1}$ and 0.20 $V·s^{-1}$ respectively.

Figure 3.40 shows the individual CV curves of CFs at scan rates of 0.01 $V·s^{-1}$, 0.05 $V·s^{-1}$, 0.07 $V·s^{-1}$, 0.08 $V·s^{-1}$, 0.10 $V·s^{-1}$, 0.12 $V·s^{-1}$, 0.15 $V·s^{-1}$ and 0.20 $V·s^{-1}$ in 5.0 mmol $K_4Fe(CN)_6$. As shown, the peak potentials (including the oxidation peak, Epa, and reduction peak, Epc) of identical electrodes at different scan rates show a negligible difference, with Epa approaching 0.35 V and Epc displaying a value of 0.17 V for the electrode sample.

Same behavior was reported by Elgrishi et al., CVs of PAN-based CFs which were performed under the same conditions as the presented in Figure 3.40[88].
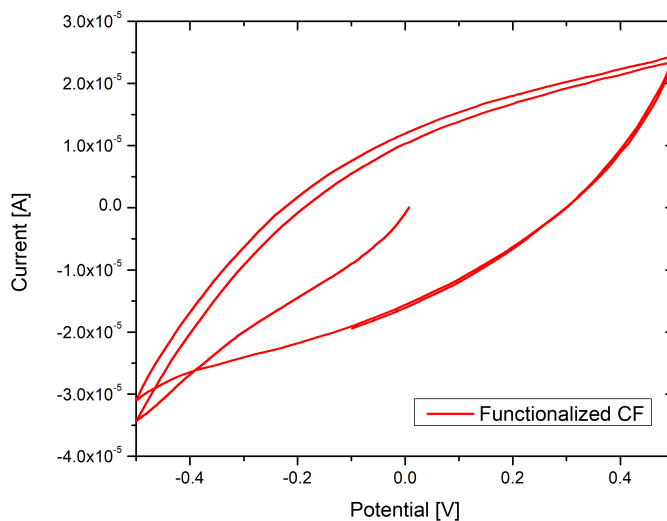
Figure 3.41: CV of a single Functionalized CF in a 5.0 mmol $K_4Fe(CN)_6$ at a scan rate of 0.1 V·s^{-1}.

The area under the voltammogram curve observed in Figure 3.41 is quite significant compared to the voltammogram of the single CF in Fig. 3.39 so the functionalization helped to have a larger surface area which translates into capacitive carbon fiber.

Subramanian et al., reported, activated carbon from banana fibers whose CV exhibit a typical capacitor behavior, and the activation process improved the porosity and increased the surface area. In contrast the BBCF shown in Figure 3.41 adjusts to their result indicating that the CV of a single Functionalized CF has a stabilized structure for a high rate capability[26].
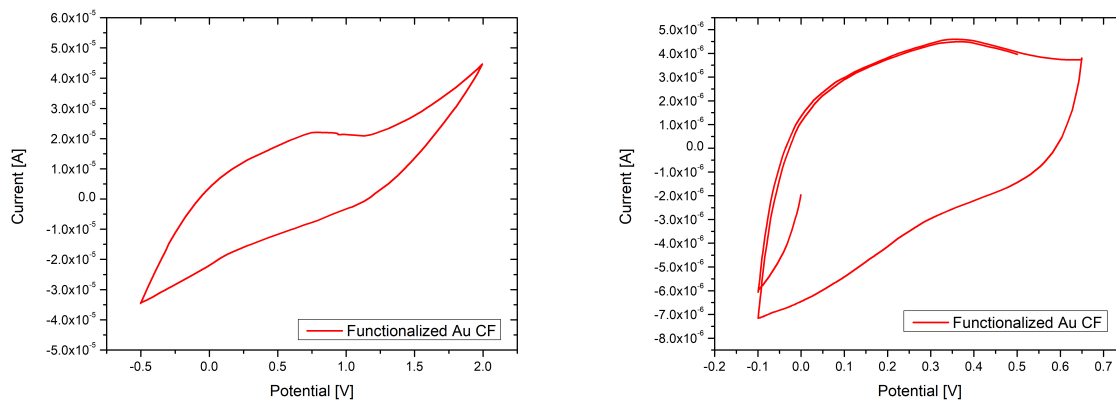
Figure 3.42: CV of a two different Functionalized CFs decorated with Au NPs in a 5.0 mmol $K_4Fe(CN)_6$ at a scan rate of 0.1 $V \cdot s^{-1}$.

The voltammograms of two different Functionalized CFs decorated with Au NPs are represented in Fig. 3.42, there the right-hand voltammogram is close to rectangular shape representing a good capacitive behavior of the electrode materials[40]. Also, the right-hand side voltammogram in Fig. 3.42 showed a slight tilt "rectangular-like shape," implying a fast charge/discharge process with high power capability and low equivalent series resistance[29].

Ruan et al, in their work "Biomass-derived carbon materials for high-performance supercapacitor electrodes", reported that due to the high content of oxygen and nitrogen functionalities in their sample, the capacitance increased significantly and the pseudo-capacitance may be a result from the heteroatom doping, which also improves the surface wettability and enhance the electronic conductivity[2]. In contrast, both Figure 3.41 and Figure 3.42 proved to have this type of behavior, as described above. Although the functionalization process decreased the amount of oxygen present in both batches (see XPS analysis, Tables 3.7 and 3.8), the level of nitrogen increased considerably due to the functionalization process, so we were facing a capacitive behavior.

Figure 3.43: Cyclic voltammogram of a pyrolyzed CF (red) and the same CF decorated with Au NPs (black) in a 1.0 M KCl at a scan rate of 0.05 V·s^{-1}.

Figure 3.43 shows the CV curves of the as-prepared CF electrode and CF decorated with Au NPs (before and after decorating) in 0.1 M KCl, performed at a scan rate of 0.05 V·s^{-1} It is observed that the single fiber has more resistance, and the area under the curve is more significant compared to the Au-decorated CF. Therefore the single CF is more capacitive, and the Au-decorated CF is more conductive.

Li et al., reported the use of AuNPs to decorate CFs as an electrode material for sensing platforms may be a viable alternative. The prepared AuNPs/CF showed excellent reproducibility and sensitivity in cyclic voltammetry [93]. In the same way BBCFs also showed this behavior.

Saw et al., recorded a CV at a scan rate of 0.025 V·s^{-1} in 0.1 M HCl of Au NPs on a a glassy carbon electrode (GCE). The Au NPs were drop cast on the GCE. They reported the presence of two little peaks: an oxidation peak at 0.85V and a reduction peak at 0.4V. Apart from this, Figure 3.43 demonstrates exactly the same behavior as that presented by Saw [102], even the same window of potential.
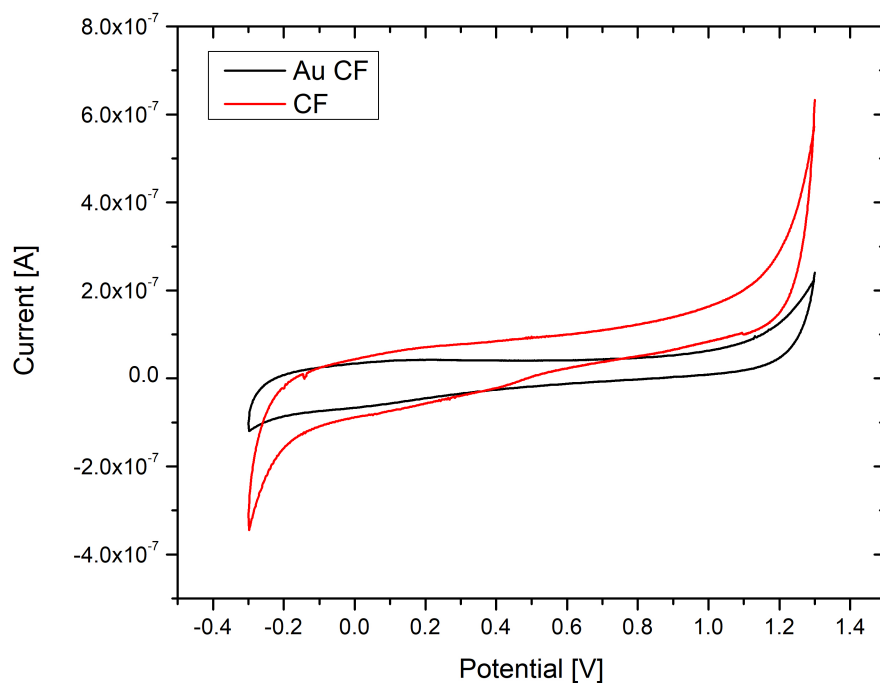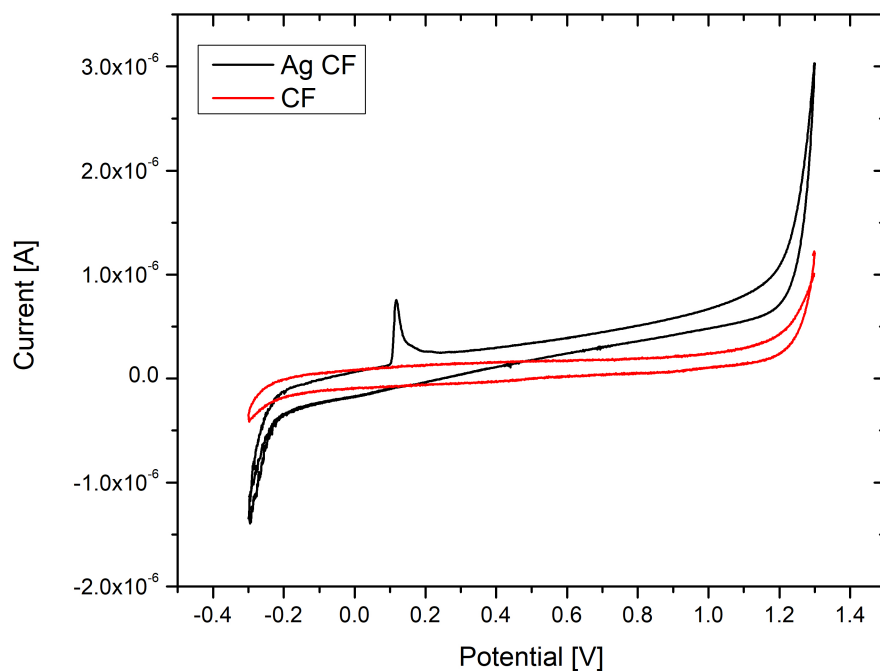
Figure 3.44: Cyclic voltammograms of a pyrolyzed CF (red) and the same CF decorated with Ag NPs (black) in a 1.0 M KCl at a scan rate of 0.05 V·s^{-1}.

Figure 3.44 shows the CV curves of the as-prepared CF electrode and CF decorated with Ag NPs (before and after decorating) in 0.1 M KCl, performed at a scan rate of 0.05 V·s^{-1}. In the voltammogram, it can be appreciated a peak belonging to the oxidation of the silver at 0.15V and also a more resistance of the CF with Ag NPs is distinguished, while the normal CF presents to be more conductive and less resistive.

Saw et al., performed electrochemical experiments of Ag NPs on a glassy carbon electrode. The Ag NPs were drop cast on the GCE. CV studies were performed in 0.1M HCl, the entire cell was placed in a Farady cage to reduce electronic noise, Cyclic voltammetry (CV) ensemble studies were performed in 0.1 M HCl (aq) in the potential range from -0.2 V to 1.2 V vs Ag/AgCl at a scan rate of 0.025 Vs^{-1} using a potentiostat (Autolab PG Stat 12). An oxidation peak was found at 0.15V and was associated to the formation of AgCl on the electrode. Then the study performed (Ag NPs on a CF) was consistent with the obtained by Saw et al[102], although they also reported the presence of a little reduction peak at -0.05V, which is not the case on the CV in Figure 3.44.

Chapter 4

Conclusions & Recommendations

4.1 Conclusions

Fibers were extracted from the banana pseudo-stem, the first batch was decorated with NPs prior to the pyrolyzation process. The second batch had a different treatment, this was first pyrolized and then functionalized and then decorated the CFs with NPs. It was demonstrated that the first batch was not suitable for the obtaining of CFs because the stem proved to be very young and therefore there was not a good amount of fibers when pyrolyzing. In contrast, the second stem which was cut after extracting the fruits of the plant and showed a very high quantity of fibers compared to the first one. This is because the tree's age influences the creation of fibers in the core of the pseudo-stem. The first stem harvested still did not show the presence of fruit. On the other hand, the second stem had already been harvested, and at the time of extracting the fibers from this last, the result was optimum.

It results in complex to obtain homogenous fibers, that is to say, to comply with the exact dimensions, and all of the fibers show the same behavior. This is because the fibers come from biomass precursors, so they are created naturally and not controlled.

Unfortunately, it is possible that the functionalized fibers suffered damages in their structure due to the fragility of the fibers. When being treated with acid for a long time, this weakened the fiber's internal structure, making it impossible to take good cyclic voltammograms.

SEM micrographs showed the presence of NPs over the surface of the functionalized carbon fibers, due to the size of CeO_2 NPs, it was complicated to obtain a good resolution of them, but the XPS and the Raman analysis confirmed the presence of them.

Raman spectroscopy results showed the structure of the fibers, how an increase of temperature was reflected into the shift of the bands, and also that at high temperatures the growth of sp2-bonded crystalline carbons increase. Also decorating the fibers with nanoparticles helped to rise the defects and disorder of the CFs.

On the other hand, XPS showed the bonds that are present in the CFs, unlike the unfunctionalized fibers, functionalized CFs had more elements present on their surface, such as N and S which are the product of the own functionalization, although also the created bonds agree with the protocol of synthesis of nanoparticles, whose

discussion is detailed in the FTIR analysis.

The FTIR spectra, as mentioned above, yielded results in which some elements were present in the CFs, and differs from the pyrolized CFs to the functionalized CFs. In this way, it must be said that the new bonds (like O-H) present in the functionalized CFs are attributed to the functionalization process.

When the cyclic voltammograms of the Functionalized and Functionalized decorated with Au NPs (Figs. 3.41 and 3.42, respectively) with the voltammogram of a single CF, Figure 3.43, were compared, it was shown that decorating and functionalization of the CFs with Au, arises into a more capacitive and the highest resistance of the electrode which is interesting for potential applications and future research on this biomass-based CFs field.

Two CVs of the gold-decorated functionalized fibers were obtain in which an entire working window was not acquired, and at the time of repeating the measurement, the fiber presented damage. This behavior is attributed to the fiber functionalization process since a single CF is too delicate even when assembling the electrode or holding it. In the process of functionalization, new functional groups could be added to the surface of the fibers and was demonstrated in the FTIR analysis, but the time of operation (the time that the CFs remained in the acidic bath) was too long, so the CFs did not respond well and at the time of performing the CVs, they did not give any signal and even break with ease. The CV analysis showed visible results in terms of the difference between the fibers functionalized with the normal fibers, in addition to the difference between decorating the fibers with nanoparticles with the fibers only pyrolyzed. Functionalized fibers proved to have a larger surface area, becoming more capacitive fibers compared to normal fibers, in addition the functionalized fibers doped with gold nanoparticles had a capacitive behavior which is not seen in the pyrolyzed fiber decorated with nanoparticles. This is because functionalized fiber had greater compatibility for nanoparticles to adhere to the surface, due to the added functional groups.

4.2   Recommendations

Due to the plant origin of the fibers, at the time of removal the fibers from the stem they will have a relatively short time until they begin to decompose, it is therefore advisable to dry the fibers in a muffle at about 65 °C to prevent them from rot and to gain a little more time to carry out the research.

The nanoparticles were present in the fibers, and the SEM corroborated it, still it is recommended to evaluate the behavior of the CFs under different decorating methods to have a more extensive view of what's the best way to decorate the fibers.

In the process of pyrolysis the temperature can be varied, as well as the previous process of treating the fibers and report the changes that the pyrolyzed fiber shows. The process of functionalization of carbon fibers is another point that must also be studied in detail due to the little existence of studies carried out on this type of material. CVs need to be repeated in order to find a good reproducibility of the electrodes behavior.

Finally, obtaining biomass-based fibers has been highly difficult, mainly due to its high fragility after the functionalization process, however it was demonstrated the technological capacity of the fibers, then it is required to perform a systematic study of the CFs.

4.3 Outlook

There is very little information related to obtaining carbon fibers from the banana pseudo-stem, the results are promising and the applications of these fibers are a field open to experimentation, from microelectrodes to supercapacitor applications and many more.

Appendix A

Reproducibility of single CF CV

Reproducibility of single CF CV with 3 different electrodes created from the same batch of fibers.
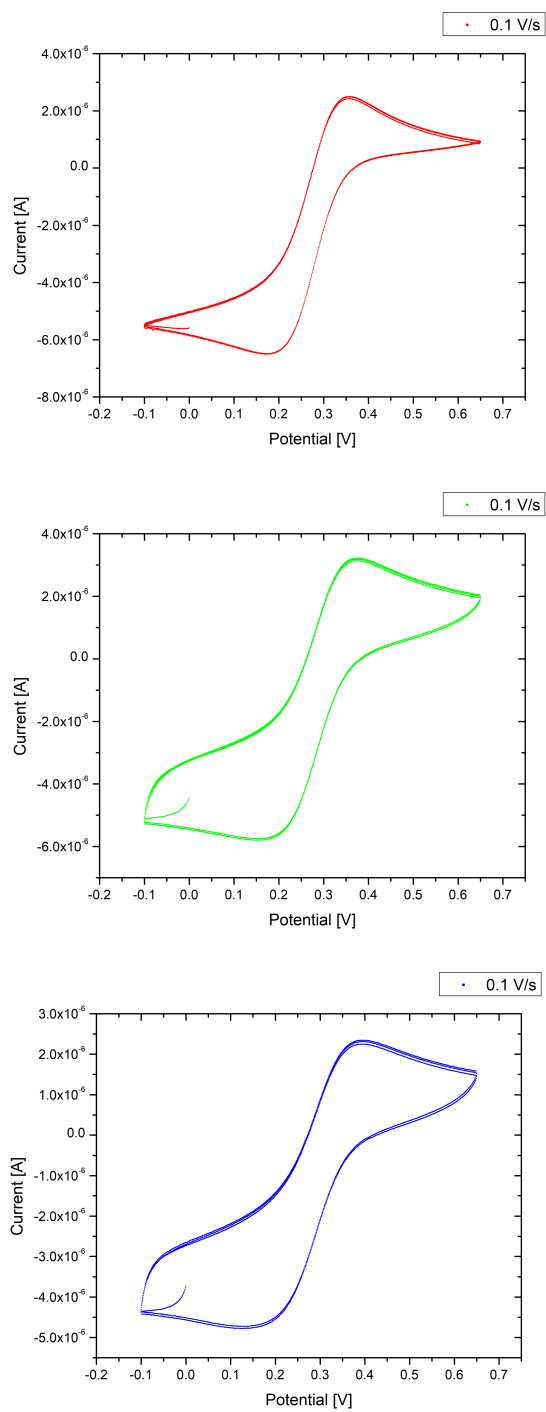
Figure A.1: Reproducibility of CVs from electrodes without treatment in a 5.0 mmol $K_4Fe(CN)_6$ at a scan rate of 0.1 V·s^{-1}.
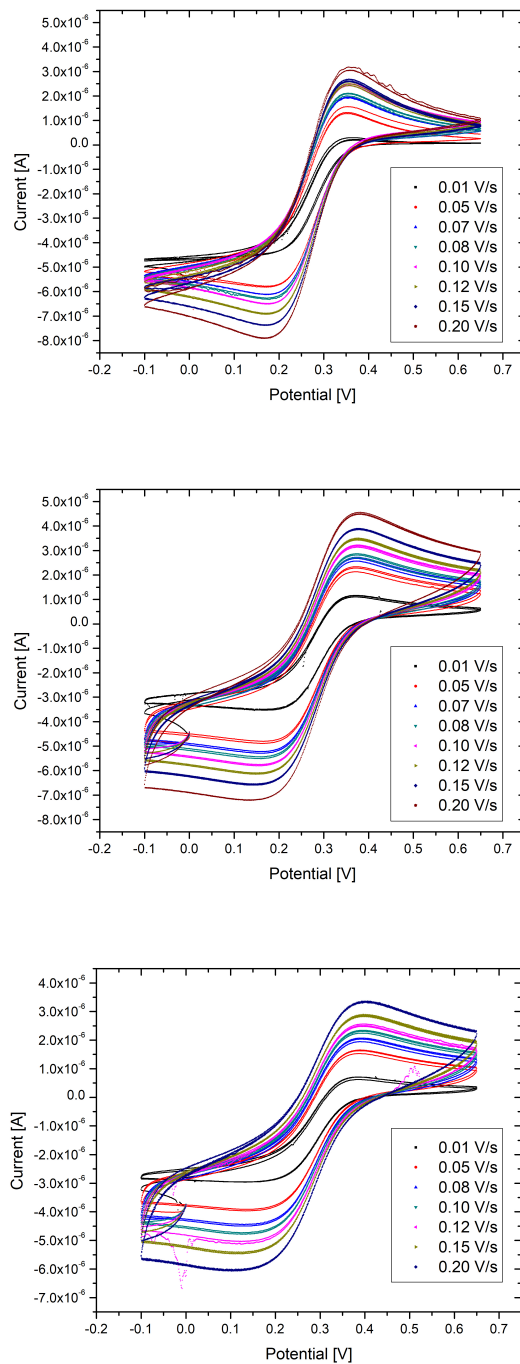
Figure A.2: CVs showing reproducibility of different electrodes without treatment at different scan rates in a 5.0 mmol $K_4Fe(CN)_6$ at a scan rate of 0.01 $V \cdot s^{-1}$, 0.05 $V \cdot s^{-1}$, 0.07 $V \cdot s^{-1}$, 0.08 $V \cdot s^{-1}$, 0.10 $V \cdot s^{-1}$, 0.12 $V \cdot s^{-1}$, 0.15 $V \cdot s^{-1}$ and 0.20 $V \cdot s^{-1}$ respectively.

Bibliography

[1] Yang, H.; Ye, S.; Zhou, J.; Liang, T. Biomass-derived porous carbon materials for supercapacitor. Frontiers in Chemistry **2019**, 7.

[2] Ruan, C.; Ai, K.; Lu, L. Biomass-derived carbon materials for high-performance supercapacitor electrodes. RSC Advances **2014**, 4, 30887–30895.

[3] Simões, F. R.; Xavier, M. G. Nanoscience and its Applications; Elsevier Inc., 2017; pp 155–178.

[4] Kalyani, P.; Anitha, A. Biomass carbon & its prospects in electrochemical energy systems. International Journal of Hydrogen Energy **2013**, 38, 4034–4045.

[5] Gao, Z.; Zhang, Y.; Song, N.; Li, X. Biomass-derived renewable carbon materials for electrochemical energy storage. 2016, 3831.

[6] Taylor, P.; Majidi, R. Molecular Physics : An International Journal at the Interface Between Chemistry and Physics A biosensor for hydrogen peroxide detection based on electronic properties of carbon nanotubes. **2013**, 37–41.

[7] Wang, J.; Wang, J.; Rogers, K. Electrochemical sensors for environmental monitoring: a review of recent technology; US Environmental Protection Agency, Office of Research and Development . . . , 1995.

[8] Nor, N. S.; Deraman, M.; Suleman, M.; Jasni, M. R.; Manjunatha, J. G.; Othman, M. A.; Shamsudin, S. A. Supercapacitors using binderless activated carbon monoliths electrodes consisting of a graphite additive and pre-carbonized biomass fibers. International Journal of Electrochemical Science **2017**, 12, 2520–2539.

[9] Baker, D. A.; Rials, T. G. Recent advances in low-cost carbon fiber manufacture from lignin. Journal of Applied Polymer Science **2013**, 130, 713–728.

[10] © FAO, Banana facts and figures. 2021; `http://www.fao.org/economic/est/est-commodities/bananas/bananafacts/en/#.XTjf0iMrI1g`.

[11] Vezina, A. Banana-producing countries . 2021; `https://www.promusa.org/Banana-producing+countries+portal`.

[12] Gonzabay, R. Cultivo del banano en el Ecuador. Revista Afese **2017**, 58.

[13] Holmes, M. Global carbon fibre market remains on upward trend. Reinforced Plastics **2014**, 58, 38–45.

[14] Frank, E.; Ingildeev, D.; Buchmeiser, M. R. Structure and Properties of High-Performance Fibers; Elsevier Ltd, 2017; Vol. 000; pp 7–30.

[15] Katepalli, H.; Bikshapathi, M.; Sharma, C. S.; Verma, N.; Sharma, A. Synthesis of hierarchical fabrics by electrospinning of PAN nanofibers on activated carbon microfibers for environmental remediation applications. Chemical Engineering Journal **2011**, 171, 1194–1200.

[16] Chang, H.; Luo, J.; Liu, H. C.; Zhang, S.; Park, J. G.; Liang, R.; Kumar, S. Carbon fibers from polyacrylonitrile/cellulose nanocrystal nanocomposite fibers. Carbon **2019**, 145, 764–771.

[17] Shindo, A. Report of the Government Industrial Research Institute; 1961.

[18] Adeniyi, A. G.; Ighalo, J. O.; Onifade, D. V. Banana and plantain fiber-reinforced polymer composites. Journal of Polymer Engineering **2019**, 39, 597–611.

[19] Chavez, E. A. Use of Natural Diatoms doped with gold nanoparticles for Gentamicin Drug Delivery; 2020.

[20] Faraday, M. X. The Bakerian Lecture. —Experimental relations of gold (and other metals) to light. Philosophical Transactions of the Royal Society of London **1857**, 147, 145–181.

[21] Ealias, A. M.; Saravanakumar, M. P. A review on the classification, characterisation, synthesis of nanoparticles and their application. IOP Conference Series: Materials Science and Engineering **2017**, 263.

[22] Hasan, S. A Review on Nanoparticles : Their Synthesis and Types. Research Journal of Recent Sciences Res . J . Recent . Sci . Uttar Pradesh (Lucknow Campus) **2014**, 4, 1–3.

[23] Machado, S.; Pacheco, J. G.; Nouws, H. P.; Albergaria, J. T.; Delerue-Matos, C. Characterization of green zero-valent iron nanoparticles produced with tree leaf extracts. Science of the Total Environment **2015**, 533, 76–81.

[24] Singh, M.; Kumar, V. LATEST ADVANCEMENTS IN CARBON BASED FIBER , A REVIEW. **2017**, 7, 327–340.

[25] Prauchner, M. J.; Pasa, V. M.; Otani, S.; Otani, C. Biopitch-based general purpose carbon fibers: Processing and properties. Carbon **2005**, 43, 591–597.

[26] Subramanian, V.; Luo, C.; Stephan, A. M.; Nahm, K. S.; Thomas, S.; Wei, B. Supercapacitors from activated carbon derived from banana fibers. Journal of Physical Chemistry C **2007**, 111, 7527–7531.

[27] Zhou, X.; Wang, P.; Zhang, Y.; Zhang, X.; Jiang, Y. From Waste Cotton Linter: A Renewable Environment-Friendly Biomass Based Carbon Fibers Preparation. ACS Sustainable Chemistry and Engineering **2016**, 4, 5585–5593.

[28] Wang, Y. Biomass-derived carbon: synthesis and applications in energy storage and conversion. 2016, 4824–4854.

[29] Du, J.; Liu, L.; Hu, Z.; Yu, Y.; Zhang, Y.; Hou, S.; Chen, A. Raw-Cotton-Derived N-Doped Carbon Fiber Aerogel as an Efficient Electrode for Electrochemical Capacitors. ACS Sustainable Chemistry and Engineering **2018**, 6, 4008–4015.

[30] Qiu, Z.; Wang, Y.; Bi, X.; Zhou, T.; Zhou, J.; Zhao, J.; Miao, Z.; Yi, W.; Fu, P.; Zhuo, S. Biochar-based carbons with hierarchical micro-meso-macro porosity for high rate and long cycle life supercapacitors. Journal of Power Sources **2018**, 376, 82–90.

[31] Zhang, L.; Tu, L. Y.; Liang, Y.; Chen, Q.; Li, Z. S.; Li, C. H.; Wang, Z. H.; Li, W. Coconut-based activated carbon fibers for efficient adsorption of various organic dyes. RSC Advances **2018**, 8, 42280–42291.

[32] Wu, T.; Li, L.; Song, G.; Ran, M.; Lu, X.; Liu, X. An ultrasensitive electrochemical sensor based on cotton carbon fiber composites for the determination of superoxide anion release from cells. Microchimica Acta **2019**, 186.

[33] Huang, X. Fabrication and properties of carbon fibers. Materials **2009**, 2, 2369–2403.

[34] Jarosz, P.; Schauerman, C.; Alvarenga, J.; Moses, B.; Mastrangelo, T.; Raffaelle, R.; Ridgley, R.; Landi, B. Nanoscale Carbon nanotube wires and cables : Near-term applications and future perspectives. 2011, 4542–4553.

[35] Xuewan Wang, P. R. D.-H. K. W. H., Gengzhi Sun; Chen, P. Heteroatom-doped graphene materials: syntheses, properties and applications. 2014,

[36] Chen, W.; Cai, S.; Ren, Q.-Q.; Wen, W.; Zhao, Y.-D. Recent advances in electrochemical sensing for hydrogen peroxide: a review. Analyst **2012**, 137, 49–58.

[37] Wang, L.; Ago, M.; Borghei, M.; Ishaq, A.; Papageorgiou, A. C.; Lundahl, M.; Rojas, O. J. Conductive Carbon Microfibers Derived from Wet-Spun Lignin/Nanocellulose Hydrogels. ACS Sustainable Chemistry and Engineering **2019**, 7, 6013–6022.

[38] Jiang, J.; Zhang, L.; Wang, X.; Holm, N.; Rajagopalan, K.; Chen, F.; Ma, S. Highly ordered macroporous woody biochar with ultra-high carbon content as supercapacitor electrodes. Electrochimica Acta **2013**, 113, 481–489.

[39] Stephan, A. M.; Kumar, T. P.; Ramesh, R.; Thomas, S.; Jeong, S. K.; Nahm, K. S. Pyrolitic carbon from biomass precursors as anode materials for lithium batteries. Materials Science and Engineering A **2006**, 430, 132–137.

[40] Uppugalla, S.; Srinivasan, P. High-performance supercapacitor coin cell: polyaniline and nitrogen, sulfur-doped activated carbon electrodes in aqueous electrolyte. Journal of Solid State Electrochemistry **2019**, 23, 295–306.

[41] Paquin, F.; Rivnay, J.; Salleo, A.; Stingelin, N.; Silva, C. Multi-phase semicrystalline microstructures drive exciton dissociation in neat plastic semiconductors. J. Mater. Chem. C **2015**, 3, 10715–10722.

[42] H. Tan, D. J. P. H. Y. S., X. Wang; Liu, H. Structural Dependent Electrode Properties of Hollow Carbon Micro-Fibers Derived from Platanus fruit and willow catkins for high-performance supercapacitors. Mater. Chem. A **2017**, 13.

[43] Zhang, L.; Zhao, X. S. Carbon-based materials as supercapacitor electrodes. Chemical Society Reviews **2009**, 38, 2520–2531.

[44] Enock, T. K.; King, C. K.; Pogrebnoi, A.; Abeid, Y.; Jande, C. Status of Biomass Derived Carbon Materials for Supercapacitor Application. **2017**, 2017.

[45] Lu, L.; Liang, L.; Teh, K. S.; Xie, Y.; Wan, Z.; Tang, Y. The electrochemical behavior of carbon fiber microelectrodes modified with carbon nanotubes using a two-step electroless plating/chemical vapor deposition process. Sensors (Switzerland) **2017**, 17, 725.

[46] Jacobs, C. B.; Peairs, M. J.; Venton, B. J. Review: Carbon nanotube based electrochemical sensors for biomolecules. Analytica Chimica Acta **2010**, 662, 105–127.

[47] Lee, J. Y.; guk Cho, D.; Cho, S. P.; Choi, J. H.; Sung, S. J.; Hong, S.; Yu, W. R. Semiconducting carbon nanotube fibers for electrochemical biosensor platforms. Materials and Design **2020**, 192, 108740.

[48] Lee, M. R.; Eckert, R. D.; Forberich, K.; Dennler, G.; Brabec, C. J.; Gaudiana, R. A. Solar power wires based on organic photovoltaic materials. Science **2009**, 324, 232–235.

[49] Donnet, J.-B.; Bansal, R. C. Carbon fibers; Crc Press, 1998.

[50] Byrne, N.; Setty, M.; Blight, S.; Tadros, R.; Ma, Y.; Sixta, H.; Hummel, M. Cellulose-Derived Carbon Fibers Produced via a Continuous Carbonization Process: Investigating Precursor Choice and Carbonization Conditions. Macromolecular Chemistry and Physics **2016**, 217, 2517–2524.

[51] Byrne, N.; De Silva, R.; Ma, Y.; Sixta, H.; Hummel, M. Enhanced stabilization of cellulose-lignin hybrid filaments for carbon fiber production. Cellulose **2018**, 25, 723–733.

[52] Chen, H.; Liu, D.; Shen, Z.; Bao, B.; Zhao, S.; Wu, L. Functional Biomass Carbons with Hierarchical Porous Structure for Supercapacitor Electrode Materials. Electrochimica Acta **2015**, 180, 241–251.

[53] Kurosaki, F.; Koyanaka, H.; Tsujimoto, M.; Imamura, Y. Shape-controlled multi-porous carbon with hierarchical micro – meso-macro pores synthesized by flash heating of wood biomass. 2008, 6, 2–9.

[54] Frank, E.; Steudle, L. M.; Ingildeev, D.; Spörl, J. M.; Buchmeiser, M. R. Carbon fibers: Precursor systems, processing, structure, and properties. Angewandte Chemie - International Edition **2014**, 53, 5262–5298.

[55] Marcuzzo, J. S.; Otani, C.; Polidoro, H. A.; Otani, S. Influence of thermal treatment on porosity formation on carbon fiber from textile PAN. Materials Research **2013**, 16, 137–144.

[56] Santiago, B. FUNCIONALIZACIÓN DE MATERIALES NANOCARBONOSOS CON POLIETIELENIMINA; pp 3–9.

[57] Ibrahim, N. A.; Fouda, M. M.; Eid, B. M. Handbook of Functionalized Nanomaterials for Industrial Applications; Elsevier, 2020; pp 581–609.

[58] Zhang, G.; Sun, S.; Yang, D.; Dodelet, J. P.; Sacher, E. The surface analytical characterization of carbon fibers functionalized by H2SO4/HNO3 treatment. Carbon **2008**, 46, 196–205.

[59] Hussain, C. M.; Keçili, R. Electrochemical techniques for environmental analysis. Modern Environmental Analysis Techniques for Pollutants **2020**, 199–222.

[60] Karimi-Maleh, H.; Karimi, F.; Alizadeh, M.; Sanati, A. L. Electrochemical Sensors, a Bright Future in the Fabrication of Portable Kits in Analytical Systems. Chemical Record **2020**, 20, 682–692.

[61] Tiwari, J. N.; Vij, V.; Kemp, K. C.; Kim, K. S. Engineered carbon-nanomaterial-based electrochemical sensors for biomolecules. ACS Nano **2016**, 10, 46–80.

[62] Chaulya, S. K.; Prasad, G. M. Gas Sensors for Underground Mines and Hazardous Areas. Sensing and Monitoring Technologies for Mines and Hazardous Areas **2016**, 161–212.

[63] Yang, C.; Denno, M. E.; Pyakurel, P.; Venton, B. J. Recent trends in carbon nanomaterial-based electrochemical sensors for biomolecules: A review. Analytica Chimica Acta **2015**, 887, 17–37.

[64] Forster, R. J.; Keyes, T. E. Handbook of Electrochemistry; Elsevier, 2007; pp 171–188.

[65] Manjavacas, G.; Nieto, B. Compendium of Hydrogen Energy; Elsevier Ltd., 2016; pp 215–234.

[66] Cross, E. S.; Lewis, D. K.; Williams, L. R.; Magoon, G. R.; Kaminsky, M. L.; Worsnop, D. R.; Jayne, J. T. Use of electrochemical sensors for measurement of air pollution: correcting interference response and validating measurements. Atmospheric Measurement Techniques Discussions **2017**, 1–17.

[67] Han, T.; Mattinen, U.; Bobacka, J. Improving the Sensitivity of Solid-Contact Ion-Selective Electrodes by Using Coulometric Signal Transduction. 2019,

[68] Jackson, D. T.; Nelson, P. N. Preparation and properties of some ion selective membranes : A review. Journal of Molecular Structure **2019**, 1182, 241–259.

[69] Pei, Y.; Hu, M.; Tang, X.; Huang, W.; Li, Z.; Chen, S.; Xia, Y. Ultrafast one-pot anodic preparation of Co 3 O 4 /nanoporous gold composite electrode as an efficient nonenzymatic amperometric sensor for glucose and hydrogen peroxide. Analytica Chimica Acta **2019**, 1059, 49–58.

[70] Guo, D.; Wu, S.; Xu, X.; Niu, X.; Li, X.; Li, Z.; Pan, J. A novel label-free hypochlorite amperometric sensor based on target-induced oxidation of benzeneboronic acid pinacol ester. Chemical Engineering Journal **2019**, 373, 1–7.

[71] Prasad, S.; Kumar, V.; Kirubanandam, S.; Barhoum, A. Emerging Applications of Nanoparticles and Architectural Nanostructures: Current Prospects and Future Trends; Elsevier Inc., 2018; pp 305–340.

[72] Behera, A.; Mallick, P.; Mohapatra, S. Corrosion Protection at the Nanoscale; Elsevier, 2020; pp 227–243.

[73] Tahir, M. B.; Rafique, M.; Rafique, M. S.; Nawaz, T.; Rizwan, M.; Tanveer, M. Nanotechnology and Photocatalysis for Environmental Applications; Elsevier, 2020; pp 119–138.

[74] Henini, M. Scanning electron microscopy: An introduction. III-Vs Review **2000**, 13, 40–44.

[75] Liu, A.; Ma, M.; Zhang, X.; Ming, J.; Jiang, L.; Li, Y.; Zhang, Y.; Liu, S. A biomass derived nitrogen doped carbon fibers as efficient catalysts for the oxygen reduction reaction. Journal of Electroanalytical Chemistry **2018**, 824, 60–66.

[76] Okuda, H.; Young, R. J.; Wolverson, D.; Tanaka, F.; Yamamoto, G.; Okabe, T. Investigating nanostructures in carbon fibres using Raman spectroscopy. Carbon **2018**, 130, 178–184.

[77] Sadezky, A.; Muckenhuber, H.; Grothe, H.; Niessner, R.; Pöschl, U. Raman microspectroscopy of soot and related carbonaceous materials: Spectral analysis and structural information. Carbon **2005**, 43, 1731–1742.

[78] Sevilla, M.; Fuertes, A. B. Direct synthesis of highly porous interconnected carbon nanosheets and their application as high-performance supercapacitors. ACS Nano **2014**, 8, 5069–5078.

[79] Karacan, I.; Erzurumluoğlu, L. The effect of carbonization temperature on the structure and properties of carbon fibers prepared from poly(m-phenylene isophthalamide) precursor. Fibers and Polymers **2015**, 16, 1629–1645.

[80] Baer, D. R.; Thevuthasan, S. Handbook of Deposition Technologies for Films and Coatings; Elsevier Inc., 2010; pp 749–864.

[81] Mather, R. R. Surface Modification of Textiles; Elsevier Inc., 2009; pp 296–317.

[82] Bagus, P. S.; Ilton, E. S.; Nelin, C. J. The interpretation of XPS spectra: Insights into materials properties. Surface Science Reports **2013**, 68, 273–304.

[83] Nie, W.; Liu, J.; Liu, W.; Wang, J.; Tang, T. Decomposition of waste carbon fiber reinforced epoxy resin composites in molten potassium hydroxide. Polymer Degradation and Stability **2015**, 111, 247–256.

[84] FTIR Spectroscopy | Equipment, Examples, Definition. `https://www.mt.com/se/sv/home/products/L1_AutochemProducts/ReactIR/ftir-spectroscopy.html`.

[85] Mondragón, P. Neural Regeneration Research; 2015; p 200.

[86] Mohamed, M. A.; Jaafar, J.; Ismail, A. F.; Othman, M. H.; Rahman, M. A. Membrane Characterization; Elsevier B.V., 2017; pp 3–29.

[87] Sandford, C.; Edwards, M. A.; Klunder, K. J.; Hickey, D. P.; Li, M.; Barman, K.; Sigman, M. S.; White, H. S.; Minteer, S. D. A synthetic chemist's guide to electroanalytical tools for studying reaction mechanisms. Chemical Science 2019, 10, 6404–6422.

[88] Elgrishi, N.; Rountree, K. J.; McCarthy, B. D.; Rountree, E. S.; Eisenhart, T. T.; Dempsey, J. L. A Practical Beginner's Guide to Cyclic Voltammetry. Journal of Chemical Education 2018, 95, 197–206.

[89] Li, W.; Qi, H.; Guo, F.; Du, Y.; Song, N.; Liu, Y.; Chen, Y. Co nanoparticles supported on cotton-based carbon fibers: A novel broadband microwave absorbent. Journal of Alloys and Compounds 2019, 772, 760–769.

[90] Yachay Tech, Equipos e Instalaciones – Yachay Tech. `https://www.yachaytech.edu.ec/geologia/geologiafacilities/`.

[91] Agilent, Flexible Benchtop FTIR Spectrometer, Cary 630 FTIR | Agilent. `https://www.agilent.com/en/product/molecular-spectroscopy/ftir-spectroscopy/ftir-benchtop-systems/cary-630-ftir-spectrometer`.

[92] Xu, J.; Yang, H.; Fu, W.; Sui, Y.; Zhu, H.; Li, M.; Zou, G. Preparation and characterization of carbon fibers coated by Fe3O4 nanoparticles. Materials Science and Engineering B: Solid-State Materials for Advanced Technology 2006, 132, 307–310.

[93] Li, D.; Li, J.; Jia, X.; Wang, E. Electrochemistry Communications Gold nanoparticles decorated carbon fi ber mat as a novel sensing platform for sensitive detection of Hg (II). Electrochemistry Communications 2014, 42, 30–33.

[94] Li, M.; Bo, X.; Mu, Z.; Zhang, Y.; Guo, L. Electrodeposition of nickel oxide and platinum nanoparticles on electrochemically reduced graphene oxide film as a nonenzymatic glucose sensor. Sensors and Actuators, B: Chemical 2014, 192, 261–268.

[95] Chen, X.; Wang, X.; Fang, D. A review on C1s XPS-spectra for some kinds of carbon materials. Fullerenes Nanotubes and Carbon Nanostructures 2020, 0, 1–11.

[96] XPS Interpretation of Carbon. `https://xpssimplified.com/elements/carbon.php`.

[97] Kim, H.-I.; Han, W.; Choi, W.-K.; Park, S.-J.; An, K.-H.; Kim, B.-J. Effects of maleic anhydride content on mechanical properties of carbon fibers-reinforced maleic anhydride-grafted-poly-propylene matrix composites. Carbon letters 2016, 20, 39–46.

[98] Perez De Berti, I. O.; Cagnoli, M. V.; Pecchi, G.; Alessandrini, J. L.; Stewart, S. J.; Bengoa, J. F.; Marchetti, S. G. Alternative low-cost approach to the synthesis of magnetic iron oxide nanoparticles by thermal decomposition of organic precursors. Nanotechnology **2013**, 24.

[99] Do, B. P. H.; Nguyen, B. D.; Nguyen, H. D.; Nguyen, P. T. Synthesis of magnetic composite nanoparticles enveloped in copolymers specified for scale inhibition application. Advances in Natural Sciences: Nanoscience and Nanotechnology **2013**, 4.

[100] Khoshnevisan, K.; Barkhi, M.; Khoshnevisan, K.; Barkhi, M.; Zare, D. Synthesis and Reactivity in Inorganic , Metal-Organic , and Nano-Metal Chemistry Preparation and Characterization of CTAB-Coated Fe 3 O 4 Nanoparticles Preparation and Characterization of CTAB-Coated Fe 3 O 4. 2011, 37–41.

[101] Zoski, C. Handbook of Electrochemistry - 1st Edition; 2006; pp 73–110.

[102] Saw, E. N.; Grasmik, V.; Rurainsky, C.; Epple, M.; Tschulik, K. Electrochemistry at single bimetallic nanoparticles - using nano impacts for sizing and compositional analysis of individual AgAu alloy nanoparticles. Faraday Discussions **2016**, 193, 327–338.